A mathematical model of the biochemical network underlying left-right asymmetry establishment in mammals

Catharine J. Roussel, Marc R. Roussel

Alberta RNA Research and Training Institute, Department of Chemistry and Biochemistry, University of Lethbridge, Lethbridge, Alberta, Canada

Abstract

The expression of the TGF-β protein Nodal on the left side of vertebrate embryos is a determining event in the development of internal-organ asymmetry. We present a mathematical model for the control of the expression of Nodal and its antagonist Lefty consisting entirely of realistic elementary reactions. We analyze the model in the absence of Lefty and find a wide range of parameters over which bistability (two stable steady states) is observed, with one stable steady state a low-Nodal state corresponding to the right-hand developmental fate, and the other a high-Nodal state corresponding to the left. We find that bistability requires a transcription factor containing two molecules of phosphorylated Smad2. A numerical survey of the full model, including Lefty, shows the effects of Lefty on the potential for bistability, and on the conditions that lead to the system reaching one or the other steady state.

Keywords: Development, Asymmetry, Mouse, Nodal, Lefty, Mathematical model

1. Introduction

The development of a left-right axis is a critical event in the development of bilaterians (Marcellini, 2006). Specification of the left-right axis is necessary to the proper development of internal organs, which are asymmetrically

Email address: roussel@uleth.ca (Marc R. Roussel)
URL: http://people.uleth.ca/~roussel (Marc R. Roussel)

distributed within the body cavity (Ramsdell and Yost, 1998). The specification of the left-right axis is a hierarchical process that can be thought of as having four major stages: (i) the initial symmetry-breaking event, (ii) the generation of an asymmetric signal, (iii) the amplification of this signal, and finally (iv) asymmetric organogenesis. The initial symmetry breaking is, at this time, poorly understood, but likely involves some very basic cellular events such as cytoskeletal reorganization following fertilization (Vandenberg and Levin, 2013). In many organisms, the generation of an asymmetric signal is widely believed to be due to a leftward flow generated by rotating cilia in the embryonic node (Nakamura and Hamada, 2012; Spéder et al., 2007), although this is still controversial (Vandenberg and Levin, 2013). Amplification of the signal involves a reaction-diffusion system whose key components are the left-determinant protein Nodal and its antagonist Lefty (Nakamura et al., 2006). The Nodal concentration is then read out by proteins such as Pitx2 to generate asymmetric organ development (Shiratori and Hamada, 2006).

This contribution focuses on the third step of this hierarchy, namely the amplification of the signal by a feedback loop involving the proteins Nodal and Lefty (Hamada et al., 2001) [or their orthologs (Schier, 2003)]. Despite the wealth of biochemical details available on this system, there has been relatively little modeling work to integrate these details and thus gain an overall understanding of the functioning of the biochemical network underlying the development of left-right asymmetry. Nakamura et al. (2006) studied a simple phenomenological model not based on detailed biochemistry. While this model yielded a great deal of insight into the potential for patterning based on the Turing mechanism (Turing, 1952), the lack of biochemical detail prevents us from drawing any firm conclusions about the *in vivo* system. Middleton et al. (2013) have studied a model that is in many ways similar to ours, arguing that "wave pinning" (a spreading wave of a particular developmental state that fails to propagate beyond a certain point) is a more likely mechanism for the amplification of the left-right asymmetry than Turing patterning. However, their model includes a Hill function to describe the kinetics of gene expression. Hill functions, because of their sigmoidal shape, often lead to nontrivial dynamics, particularly for larger values of the Hill coefficient, so the question naturally arises as to whether the results are an artifact of the Hill activation kinetics.

One objective of this paper is to generate a model that contains a reasonable level of biochemical detail expressed fully in terms of realistic chemical

reactions, avoiding empirical rate laws such as Michaelis-Menten or Hill functions. Except in very simple cases, an empirical rate law raises the question of how such a rate law might have arisen. By choosing reactions that are supported by the experimental evidence, if sometimes in simplified form, we avoid a model whose behavior is dependent on a particular assumed rate law. Another advantage is that we can deploy powerful tools developed to analyze models in mass-action form.

In this paper, we focus on the behavior of a single cell, leaving spatio-temporal behavior to a later paper. Lewis et al. (1977) argued long ago that developmental events are likely determined either by bistable kinetics, with two stable steady states representing different developmental fates, or by bifurcations changing the qualitative pattern of gene expression. In a system in which we observe two distinct gene expression patterns, one associated with the left-hand fate, and one with the right, bistability is certainly an attractive hypothesis. Bistable systems are often capable of sustaining wave activity, i.e. of causing a particular state to spread (Rinzel and Terman, 1982). All that is then needed is a mechanism to stop the wave, of which several have been investigated (Keener, 1987; Matthies and Wayne, 2006; Mori et al., 2008). Furthermore, the necessary structural requirements on a chemical network to allow Turing bifurcations coincide with those for oscillations or bistability in a spatially homogeneous model (Mincheva and Roussel, 2006, 2007). Bistable kinetics thus allows for multiple mechanisms of patterning. An understanding of the cell-autonomous behavior therefore sets up later studies of the spatio-temporal behavior.

The plan of the paper is as follows: In section 2, we describe our model. Throughout this section, we emphasize known biochemical reactions or, at the very least, reactions supported by some amount of experimental evidence. Although the biochemistry is very similar in all vertebrates, we focus on observations in mice whenever possible. Prior to presenting our analysis, we briefly introduce some ideas and terminology from nonlinear dynamics in section 3.1 for those readers not familiar with this field. Section 3.2 describes graph-theoretical methods we later use for qualitative stability analysis. Section 4 presents an analysis of a minimal bistable subnetwork involving Nodal only. We note the intriguing recent observation that feedback from Lefty is not necessary for appropriate left-right development in zebrafish (Rogers et al., 2017), which partially motivates this study. In section 5, we carry out a study of the full model, emphasizing the effect of Lefty-related reactions on the qualitative behavior of the model, as well as quantitative effects on the

set of initial conditions that allow a cell to reach a desired steady state. We also find that the Nodal-Lefty network admits oscillatory solutions. Finally, in section 6, we offer some closing observations and conclusions.

2. The Model

The biochemical network that amplifies the initial asymmetric signal is similar, but not identical, across species (Capdevila et al., 2000; Nakamura and Hamada, 2012). For the purposes of this model, we have emphasized biochemical studies in mice, the most heavily studied mammalian model organism.

Figure 1 illustrates the key features of the model we are exploring. At the cellular level, externally circulating Nodal induces the production of both Nodal itself and its inhibitor Lefty by binding to TGF-β receptors at the cell surface (Hamada et al., 2001). The binding of Nodal to the receptor promotes the phosphorylation of Smad2, which dimerizes with itself, and then forms a complex with Smad4 (Massagué et al., 2005; Hill, 2016). This heterotrimer is part of a transcription factor that activates the transcription of the *nodal* and *lefty* genes. Lefty inhibits Nodal signaling both by competition for the cell-surface receptor and by uncompetitive binding to the Nodal-receptor complex (Ulloa and Tabibzadeh, 2001).

2.1. Ligand-receptor kinetics

Nodal assembles a complex that includes type I and type II TGF-β receptors (Acvr1b, and Acvr2a or 2b) (Massagué et al., 2005; Shen, 2007; Ross and Hill, 2008; Hill, 2016) at the cell surface with the assistance of the co-receptor Cripto (Reissmann et al., 2001; Sakuma et al., 2002). For simplicity, we model this as a single binding event to a receptor R that activates the latter's kinase activity. This will be a reasonable approximation to the more complex interplay between Nodal, Cripto and the TGF-β receptors provided the assembly process has a single rate-determining step.

$$\mathrm{N_e} + \mathrm{R} \underset{k_{-1}}{\overset{k_1}{\rightleftharpoons}} \mathrm{R_A}. \tag{1}$$

In this reaction, $\mathrm{N_e}$ represents extracellular Nodal, and $\mathrm{R_A}$ is the activated receptor.

In mammals, there are two Lefty proteins, called Lefty1 and Lefty2 in mice (Hamada et al., 2001). The two Lefties have identical antagonistic

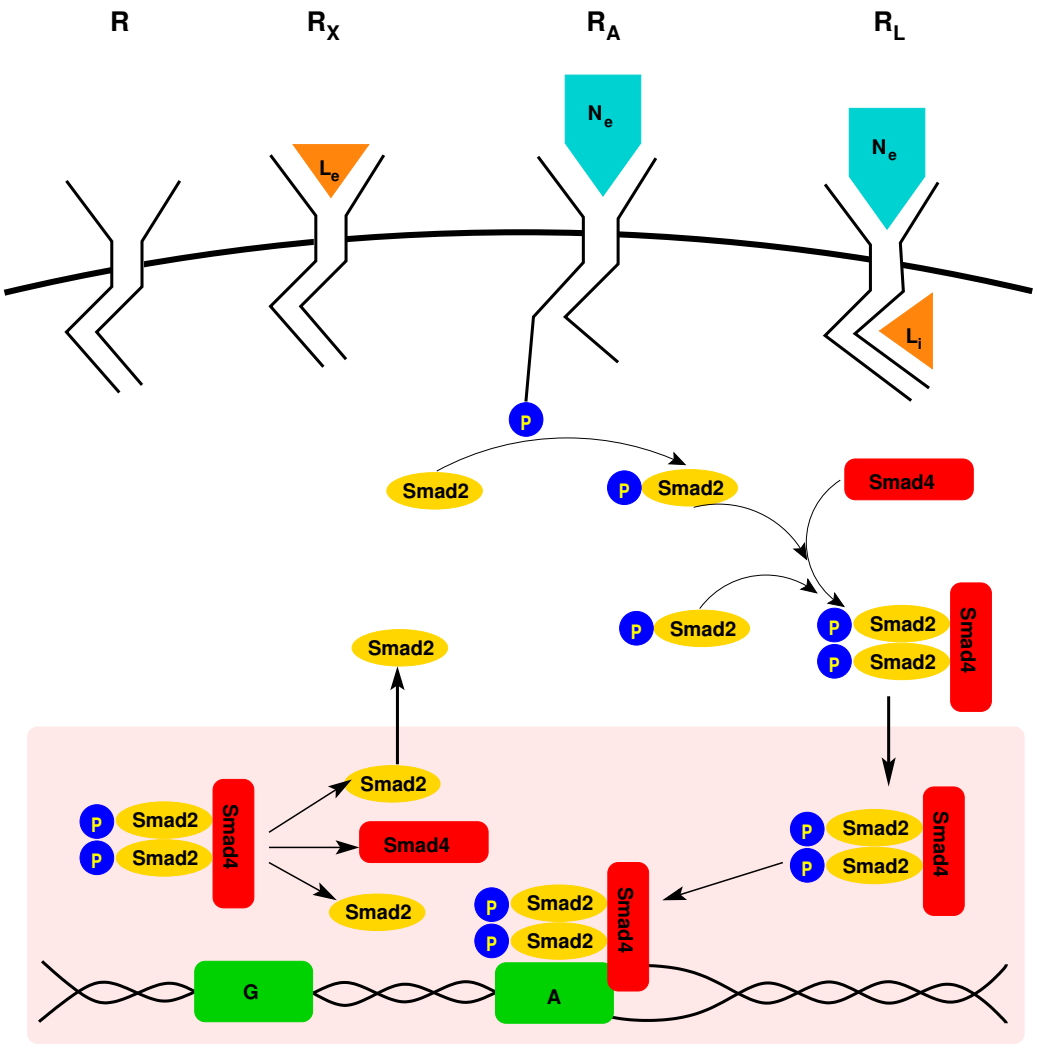

Figure 1: Major biochemical interactions included in the model. Extracellular Nodal (N_e) binds to the Acvr1b/Acvr2b receptor complex (R) on the surface of the cell. The Nodal-receptor complex (R_A) is a kinase that phosphorylates Smad2. Phosphorylated Smad2 proteins dimerize and combine with Smad4 to create a transcription factor that binds to the promoter sites of both Nodal and Lefty genes to activate their transcription. In this figure, G represents one of the Nodal or Lefty gene promoters, and A a promoter activated by the transcription factor. Extracellular Lefty (L_e) competes with Nodal for receptor binding sites, forming an inactive complex (R_X). Uncompetitive binding of intracellular Lefty (L_i) to the Nodal-bound receptor also results in an inactive complex (R_L).

effects on Nodal signaling (Shiratori and Hamada, 2014). However, their expression is differently regulated and they have different developmental roles (Meno et al., 1998; Juan and Hamada, 2001). We focus here on Lefty2, which is involved in a feedback loop with Nodal (Meno et al., 1999) to determine the left side of the embryo (Hamada et al., 2001). Accordingly, we use the terms Lefty and Lefty2 interchangeably. Extracellular Lefty2 (L_e) binds competitively to the receptor, inhibiting Nodal activation of the transcription of both Nodal and Lefty2 (Meno et al., 1999; Sakuma et al., 2002; Cheng et al., 2004; Chen and Shen, 2004; Shiratori and Hamada, 2014).

$$L_e + R \underset{k_{-2}}{\overset{k_2}{\rightleftharpoons}} R_X, \tag{2}$$

where R_X is an inactive receptor complex. We note that this is not a fully biochemically realistic description of the inhibition mechanism, which likely involves binding of Lefty to the coreceptor Cripto (Cheng et al., 2004; Chen and Shen, 2004). However, the essence of the interaction, competitive inhibition of Nodal signaling by Lefty, is preserved in this simplified representation.

The cytoplasmic receptor-activated Smads (R-Smads), Smad2 and Smad3, have both similar and divergent roles in development (Alvarez and Serra, 2004; Brown et al., 2007). They are both phosphorylated by the Nodal-activated receptors (Souchelnytskyi et al., 1997; Schier, 2009) and are thought to be interchangeable in the development of left-right asymmetry. We therefore consider a single R-Smad, which we denote Smad2 for simplicity. Activation of Smad2 by phosphorylation is an essential step in the transduction of the Nodal signal (Souchelnytskyi et al., 1997; Besser, 2004; Ross and Hill, 2008). Smad3 has been shown to be phosphorylated at the cell surface (Li et al., 2016), and we assume this is the case for both R-Smads. Following Middleton et al. (2013), we ignore any steps required to recharge the receptor with phosphate and assume that it behaves like a simple Michaelian enzyme:

$$R_A + \mathrm{Smad2} \underset{k_{-3}}{\overset{k_3}{\rightleftharpoons}} R_A S_2, \tag{3}$$

$$R_A S_2 \xrightarrow{k_4} \mathrm{PSmad2} + R_A, \tag{4}$$

where $R_A S_2$ is the enzyme-substrate complex, and PSmad2 is the phosphorylated R-Smad.

In vivo, dephosphorylation of Smad2 plays a key role in the nucleocytoplasmic shuttling of this species (Massagué et al., 2005; Schmierer et al.,

2008). We do not explicitly consider the compartmentalization of the cell in our model, but discovered in the course of studying the model's behavior that including dephosphorylation of Smad2,

$$\text{PSmad2} \xrightarrow{k_5} \text{Smad2}, \tag{5}$$

was essential to the structural stability of the model. (See section 3.1 for a definition of structural stability and section 4.1 for the calculations leading to this conclusion.)

Nodal trafficking likely involves two routes for internalization, one coupled to signaling and one leading to degradation (Constam, 2009; Schier, 2009). Internalized Nodal may consist of two distinct pools, one of which may be excreted (Constam, 2009), although some evidence suggests that this process is irreversible (Le Good et al., 2005). These processes are beyond the scope of the current model, which focuses on Nodal signal transduction and its inhibition by Lefty. Accordingly, we consider a single reversible internalization process for each of Nodal and Lefty.

$$\mathrm{N_e} \underset{k_{-6}}{\overset{k_6}{\rightleftharpoons}} \mathrm{N_i}, \tag{6}$$

$$\mathrm{L_e} \underset{k_{-7}}{\overset{k_7}{\rightleftharpoons}} \mathrm{L_i}, \tag{7}$$

where the subscripts 'i' indicate the internalized species.

In addition to direct competition for the receptor by extracellular Lefty [reaction (2)], Lefty inhibits phosphorylation of Smad2 downstream of receptor activation by extracellular Nodal [reaction (1)] (Ulloa and Tabibzadeh, 2001). For simplicity, we assume here uncompetitive inhibition (binding of $\mathrm{L_i}$ exclusively to the activated receptor $\mathrm{R_A}$), although noncompetitive inhibition (binding to any state of the receptor) would also be consistent with the experimental observations of Ulloa and Tabibzadeh (2001).

$$\mathrm{R_A} + \mathrm{L_i} \underset{k_{-8}}{\overset{k_8}{\rightleftharpoons}} \mathrm{R_L}. \tag{8}$$

Here, $\mathrm{R_L}$ represents another inactive form of the receptor.

2.2. Transcriptional control

The phosphorylated R-Smads form homodimers (Hill, 2016):

$$2\ \text{PSmad2} \underset{k_{-9}}{\overset{k_9}{\rightleftharpoons}} (\text{PSmad2})_2. \tag{9}$$

Some evidence suggests that the Smad2 transcription factor complex consists of two phosphorylated Smad2 units with one unit of the Smad4 cofactor (Inman and Hill, 2002). We assume that this complex is assembled from the PSmad2 dimers, although other assembly pathways are possible, and may operate instead of or in parallel with this one. (A qualitative analysis (not shown) suggests that the dynamics are not sensitive to this order.) Assembled in the cytoplasm, the Smad ternary complex travels to the nucleus where it remains (Schmierer et al., 2008). The Smad complex associates with additional factors not considered explicitly in this model (e.g. FoxH1) to form a transcription factor, TF (Massagué et al., 2005; Hill, 2016). We summarize these processes with the single, highly simplified reaction

$$(\mathrm{PSmad2})_2 + \mathrm{Smad4} \xrightarrow{k_{10}} \mathrm{TF}. \tag{10}$$

We note briefly that the stoichiometry of the PSmad3-Smad4 transcription factor complex may be 1:1 (Inman and Hill, 2002). We do not consider the possibility that Smad2 and Smad3 provide alternative transcriptional activation pathways with complexes of differing stoichiometries, although we do examine the dynamical consequences of reducing the stoichiometry of the phosphorylated R-Smad in the transcription factor to one unit in section 4.2.

Dephosphorylation of Smad2 within the complex results in its dissassembly. The component parts are then exported to the cytoplasm. Again, for simplicity, we represent this complex process by the single reaction

$$\mathrm{TF} \xrightarrow{k_{11}} 2\ \mathrm{Smad2} + \mathrm{Smad4}. \tag{11}$$

The transcription factor activates both the *nodal* ($\mathrm{G_N}$) and *lefty* ($\mathrm{G_L}$) genes. The activated genes are denoted, respectively, $\mathrm{A_N}$ and $\mathrm{A_L}$. Thus, the activation process for the *nodal* gene can be written

$$\mathrm{TF} + \mathrm{G_N} \underset{k_{-12}}{\overset{k_{12}}{\rightleftharpoons}} \mathrm{A_N}. \tag{12}$$

Nodal is initially synthesized as a preprotein, which is cleaved to the fully active form as it is exported from the cell (Blanchet et al., 2008; Tessadori et al., 2015). Moreover, the mature Nodal proteins form homodimers. We combine these processes into a single effective reaction producing (implicitly) dimeric extracellular Nodal:

$$\mathrm{A_N} \xrightarrow{k_{13}} \mathrm{A_N} + \mathrm{N_e}. \tag{13}$$

If we only include the reactions above, in the absence of Nodal signaling, there is a steady state with zero concentrations of Nodal and Lefty. This is probably not realistic as there is always some level of leaky gene expression, captured by the following reaction:

$$\mathrm{G_N} \xrightarrow{k_{14}} \mathrm{G_N} + \mathrm{N_e}. \tag{14}$$

In a similar fashion, the transcription factor binds to and activates the *lefty* gene:

$$\mathrm{TF} + \mathrm{G_L} \underset{k_{-15}}{\overset{k_{15}}{\rightleftharpoons}} \mathrm{A_L}. \tag{15}$$

Lefty is similarly synthesized as a preprotein, which is then processed into an active form (Meno et al., 1996; Ulloa et al., 2001). By analogy to Nodal, and lacking information to the contrary, we assume that Lefty is processed and exported concurrently, leading to the overall synthesis process

$$\mathrm{A_L} \xrightarrow{k_{16}} \mathrm{A_L} + \mathrm{L_e}. \tag{16}$$

We again include the possibility of leaky gene expression:

$$\mathrm{G_L} \xrightarrow{k_{17}} \mathrm{G_L} + \mathrm{L_e}. \tag{17}$$

2.3. Protein degradation

Lefty and Nodal undergo extracellular degradation (Müller et al., 2012):

$$\mathrm{N_e} \xrightarrow{k_{18}} \emptyset, \tag{18}$$

$$\mathrm{L_e} \xrightarrow{k_{19}} \emptyset. \tag{19}$$

Although internalized Nodal does not appear to have a specific role in Nodal signaling, it is known to be rapidly degraded (Le Good et al., 2005; Constam, 2009). Accordingly, internalization acts as a sink for Nodal and is included in the model for this reason.

$$\mathrm{N_i} \xrightarrow{k_{20}} \emptyset. \tag{20}$$

Since both Nodal and Lefty are members of the TGF-β family, we assume that they have similar degradation kinetics once internalized:

$$\mathrm{L_i} \xrightarrow{k_{21}} \emptyset \tag{21}$$

Table 1 provides a full list of the species appearing in the model.

Table 1: Chemical species appearing in the model

Symbol	**Meaning**
N_e	Extracellular Nodal
N_i	Intracellular Nodal
L_e	Extracellular Lefty
L_i	Intracellular Lefty
R	Free receptor
R_A	Receptor activated by Nodal binding
R_AS_2	Enzyme-substrate complex in phosphorylation of Smad2 by R_A
R_X	Receptor inactivated by binding of extracellular Lefty
R_L	Inactive receptor bound to extracellular Nodal and to intracellular Lefty
Smad2	Lumped species representing the R-Smads Smad2 and Smad3
PSmad2	Phosphorylated Smad2/3
$(Psmad2)_2$	PSmad2 dimer
Smad4	Co-Smad Smad4
TF	Transcription factor
G_N	Bare *nodal* gene promoter
A_N	*nodal* promoter activated by TF binding
G_L	Bare *lefty* gene promoter
A_L	*lefty* promoter activated by TF binding

3. Mathematical background

3.1. Terminology from nonlinear dynamics

For readers less familiar with the techniques of nonlinear dynamics, we present here a brief introduction to some of the relevant ideas, which should be sufficient to follow the arguments presented in subsequent sections of this paper. Many excellent textbooks cover this material in greater depth, including Glass and Mackey (1988), Goldbeter (1996), Murray (2002) and Strogatz (1994), to name just a few.

The set of independent variables (concentrations of chemical species, denoted here by x_i) in a model define a **phase space**. The time evolution of a system can be thought of as a trajectory in phase space.

For sufficiently small displacements from a steady state (equilibrium point), the rate equations can be approximated by linear differential equations. The solutions of linear differential equations are superpositions of exponential terms $e^{\lambda_i t}$. The λ_i are known as **eigenvalues** because of their connection to a matrix eigenvalue problem. If the real parts of the eigenvalues at a given steady state are all negative, then that steady state is **locally stable**, i.e. trajectories started from nearby points in phase space will be attracted to the steady state. On the other hand, if any of the eigenvalues has a positive real part, then the steady state is **locally unstable**, and trajectories started nearby will eventually escape the neighborhood of this steady state. If all the eigenvalues are real and of the same sign, then the steady state is a **node**, which may be stable or unstable. If there is at least one pair of complex eigenvalues, especially if those eigenvalues are those with the smallest real parts, corresponding to the slowest mode of motion in the linearized picture, the steady state is a **focus**, and we can again have stable or unstable foci. A steady state with both positive and negative eigenvalues is called a **saddle point**.

When there is more than one stable steady state, each has its own **basin of attraction**, a region of phase space within which the system evolves toward the steady state it contains.

Negative eigenvalues are associated with directions (eigenvectors) along which the steady state is approached. A trajectory (or set of trajectories) that enters the steady state along one of these stable directions is called a **stable manifold**. Similarly, positive eigenvalues are associated with repelling directions. A trajectory that leaves a steady state along one of these directions is an **unstable manifold**.

A trajectory that connects an unstable steady state to itself is called a **homoclinic orbit**. A homoclinic orbit leaves the steady state along its unstable manifold, and reenters along the stable manifold. A trajectory that connects an unstable steady state to another steady state is called a **heteroclinic orbit**. A heteroclinic orbit leaves one steady state along its unstable manifold, and enters the other along its stable manifold.

The eigenvalues are solutions of a **characteristic polynomial**, which can be written in the form

$$\lambda^r + c_1\lambda^{r-1} + \ldots + c_{r-1}\lambda + c_r = 0. \tag{22}$$

The coefficients c_i depend on the parameters of the model. In the case where a model has multiple steady states for a given set of parameters, each steady state will have its own characteristic polynomial. For a (bio)chemical system, r is the rank of the stoichiometry matrix. In writing Eq. (22), we have assumed that any available conservation relations (e.g. enzyme conservation, or conservation of gene promoters) have been used to eliminate a corresponding number of variables. For a (bio)chemical system, r is then both the number of independent differential equations, and the rank of the stoichiometric matrix. If the available conservation relations are not used, then an extra factor of λ^n can be removed from the characteristic polynomial, where n is the number of conservation relations, leaving us once again with Eq. (22).

A **bifurcation** is a qualitative change in the solutions of a set of differential equations when we change (in the simplest case) one parameter of the model. In a **saddle-node bifurcation**, a stable and an unstable steady state collide and are annihilated. A **transcritical bifurcation** also involves a collision between a stable and an unstable steady state, but in this case, the two steady states pass through each other, exchanging stability as they do so. Both saddle-node and transcritical bifurcations occur when the constant term of the characteristic polynomial, c_r, passes through zero.

Complex eigenvalues come in complex-conjugate pairs and correspond to oscillatory modes. An **Andronov-Hopf bifurcation** (frequently known simply as a Hopf bifurcation) involves a change in sign of the real part of a complex-conjugate pair of eigenvalues. In the simplest case (a **supercritical** Andronov-Hopf bifurcation), a steady state loses stability when the real parts of a complex-conjugate pair become positive and a stable oscillatory solution known as a (stable) **limit cycle** is born in the process. In a **subcritical** Andronov-Hopf bifurcation, an unstable limit cycle shrinks down around a

stable steady state, causing the steady state to lose stability when the radius of the limit cycle shrinks to zero.

A more subtle type of bifurcation involves a collision of a limit cycle with a saddle point, known as a **homoclinic bifurcation**, leading to disappearance of the limit cycle (Hale and Koçak, 1991). At the parameter value where the collision occurs, the limit cycle becomes a homoclinic orbit of the saddle point. Because the saddle point is an equilibrium point and the rates of change of the variables are small in the vicinity of this point, the period diverges to infinity as the limit cycle approaches the saddle point, which is diagnostic of a homoclinic bifurcation.

Because no model ever includes all possible reactions and chemical species, the behavior of a useful model should be robust to the addition of "small" terms to the rate equations, at least within some class of small terms that is relevant to the system being studied (Andronov and Pontrjagin, 1937). This property is called **structural stability** (Thom, 1975).

3.2. Graph-theoretical analysis

For a large model such as the one studied here, a full analytic study of the characteristic polynomial is rarely possible. However, qualitative methods based on an analysis of the structure of the model, abstracted from particular parameter values, can yield insights complementary to those obtained from numerical methods. Qualitative methods have a long history (Quirk and Ruppert, 1965; Feinberg, 1987; Thomas and Kaufman, 2001). Here we will use a method first developed by Ivanova (1979) based on some earlier work of Clarke (1974). Additional details on the use of this method are available from Ermakov and Goldstein (2002), Ermakov (2003), Goldstein et al. (2004), and Mincheva and Roussel (2007).

In Ivanova's method, a mass-action reaction mechanism is first represented as a **bipartite graph**, with one set of vertices representing chemical species (S_i), and the other reactions (R_i). The graph is constructed by drawing arrows from reactant species to reaction vertices, and from reactions to product species. For example, the following is the bipartite graph of reaction (1):

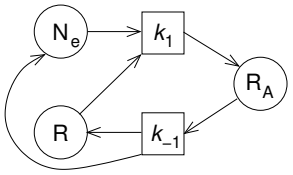

The two types of vertices are represented by different shapes, here circles for species and squares for reactions, the latter represented by their respective rate constants. The two directions of a reversible reaction are treated as different reactions, as shown above. The weight of an arrow is the corresponding stoichiometric coefficient. Implicitly, all arrows have a weight of 1 unless otherwise shown by placing the weight over the arrow. The bipartite graph of the entire mechanism is drawn as a basis for the subsequent analysis.

A **subgraph** consists of a set of mutually disjoint edges and cycles. An **edge**, denoted $[\mathrm{S}_i, \mathrm{R}_j]$, is a reactant (not product) vertex connected by an arrow to a reaction vertex. A **cycle** can be constructed of two kinds of paths from a species vertex through a reaction vertex to another species vertex: A **positive path**, denoted $[\mathrm{S}_i, \mathrm{R}_j, \mathrm{S}_k]$ starts at a reactant, goes through a reaction, and ends at a product of the reaction. A **negative path**, $\overline{[\mathrm{S}_i, \mathrm{R}_j, \mathrm{S}_k]}$ starts at a reactant, goes through a reaction, and then follows an arrow backwards to a different reactant of the same reaction. A **fragment** is the set of all subgraphs that can be made from a common set of species and reaction vertices. The number of species vertices in a fragment is its **order**. The connection to stability analysis is that a fragment of order k corresponds to a term in the coefficient c_k of the characteristic polynomial. Moreover, the coefficient of the corresponding term can be calculated from the structure of the fragment as follows: Each cycle C has a coefficient

$$K_C = \prod_{\overline{[\mathrm{S}_i,\mathrm{R}_j,\mathrm{S}_k]}\in C} (-\alpha_{ji}\alpha_{jk}) \prod_{[\mathrm{S}_i,\mathrm{R}_j,\mathrm{S}_k]} \alpha_{ji}\beta_{jk}, \tag{23}$$

where α_{ji} is the stoichiometric coefficient of reactant i in reaction j (weight of the arrow from S_i to R_j), and β_{jk} is the stoichiometric coefficient of product k in reaction j (again, the weight of the corresponding arrow in the bipartite graph). Each subgraph G has a coefficient

$$K_G = (-1)^{t_G} \prod_{[\mathrm{S}_i,\mathrm{R}_j]\in G} \alpha_{ji}^2 \prod_{C\in G} K_C, \tag{24}$$

where t_G is the number of cycles in the subgraph. Finally, if we denote a fragment by S_k, where k is the order of the fragment, then the coefficient of a fragment, which coincides with a coefficient of the corresponding term in the characteristic polynomial, is given by

$$K_{S_k} = \sum_{G\in S_k} K_G. \tag{25}$$

A **critical fragment** is a fragment with a negative coefficient. Software for critical fragment identification is available (Walther et al., 2014). The importance of a critical fragment is clear for bistability: A saddle-node bifurcation occurs when the constant term in the characteristic polynomial, c_r, is zero. If all the terms in c_r are positive, then it is impossible to have a saddle-node bifurcation. Conversely, a critical fragment of order r is a necessary condition for the existence of a saddle-node bifurcation. This condition is not sufficient, but in our experience, it is unusual not to be able to find parameters resulting in bistability in a model with a critical fragment of order r.

For the Andronov-Hopf bifurcation, the situation is more delicate. Suppose that, for some set of parameters $\mathcal{P}_1$ and for one particular steady state, all of the coefficients of the characteristic polynomial are positive, and that moreover this steady state is stable, i.e. all of the eigenvalues have negative real parts. It is known that if, through a change in the parameters to a second set $\mathcal{P}_2$, one of the c_k can be made negative for any $k < r$, then the steady state will be unstable (Ivanova and Tarnopol'skii, 1979). It follows that an instability, as it turns out of the Andronov-Hopf type, will set in for some parameter values between $\mathcal{P}_1$ and $\mathcal{P}_2$. Starting from a characteristic polynomial with all positive coefficients, since one of the coefficients has become negative at $\mathcal{P}_2$, this means that this coefficient needs to decrease to reach the Andronov-Hopf bifurcation. Accordingly, we again need a negative term, this time in c_k, in order for it to be possible to reach the bifurcation. A negative term in c_k occurs only if there is a critical fragment of order k. Then it may be possible to adjust the parameters in such a way as to make this negative term sufficiently large to reach the Andronov-Hopf bifurcation. Again, the existence of a critical fragment is necessary but not sufficient, but also our experience shows that it is generally possible to find an Andronov-Hopf bifurcation in models possessed of a critical fragment of order $k < r$.

4. Nodal-only model

The autocatalytic Nodal subsystem, leaving out Lefty altogether, is able to generate bistability of itself, as has frequently been seen in systems with autocatalysis (Edelstein, 1970; Goldbeter, 1996; Mackey et al., 2016). Moreover, a recent experimental study in zebrafish suggests that Lefty may not be required for patterning, and may instead play a role in modulating the concentration of Nodal (Rogers et al., 2017). That being the case, we initially

focus on a (roughly) minimal bistable system, which consists of reactions (1), (3)–(5), (9)–(13) and (18) with $k_{-3} = k_{-9} = 0$. The latter two rate constants were set to zero because doing so did not break any cycles in the model, and the structural stability of the model means that it will be possible to retain any given behavior when nonzero values are reintroduced. Understanding the basic circuitry leading to bistability will then help us understand the potential role of Lefty.

4.1. Core bistable model

The inclusion in the model of interactions at gene promoters [reactions (12) and, in the full model, (15)] means that we should, in principle use a Markov model to treat these interactions, given the small copy numbers of the relevant genes (two for each gene in a diploid cell). This would introduce a random element in the model. Given that this is a new model, we want to focus on the dynamics of the system, from which a great deal can be learned, and avoid stochastic effects, as interesting as those may prove to be in the longer term. Accordingly, we use differential equations to model all of the concentrations. The reaction rate terms involving low-abundance species, in particular the genes, should therefore be thought of as mean-field terms, i.e. averages over a large ensemble of cells. Thus, we could think of this model as one that could describe directly *in vitro* experiments with cultured cells, all of which receive the same treatment. Moreover, the rate constants appearing in the model are ordinary mass-action rate constants that could be measured in bulk biochemical experiments using purified components.

Using the law of mass action, we derive the following equations governing the core bistable Nodal subsystem:

$$\frac{d[\mathrm{N_e}]}{dt} = -k_1[\mathrm{N_e}][\mathrm{R}] + k_{-1}[\mathrm{R_A}] + k_{13}[\mathrm{A_N}] - k_{18}[\mathrm{N_e}], \tag{26}$$

$$\frac{d[\mathrm{R_A}]}{dt} = k_1[\mathrm{R}][\mathrm{N_e}] - k_{-1}[\mathrm{R_A}] - k_3[\mathrm{R_A}][\mathrm{Smad2}] + k_4[\mathrm{R_AS_2}], \tag{27}$$

$$\frac{d[\mathrm{R_AS_2}]}{dt} = k_3[\mathrm{R_A}][\mathrm{Smad2}] - k_4[\mathrm{R_AS_2}], \tag{28}$$

$$\frac{d[\mathrm{PSmad2}]}{dt} = k_4[\mathrm{R_AS_2}] - k_5[\mathrm{PSmad2}] - 2k_9[\mathrm{PSmad2}]^2, \tag{29}$$

$$\frac{d[(\mathrm{PSmad2})_2]}{dt} = k_9[\mathrm{PSmad2}]^2 - k_{10}[(\mathrm{PSmad2})_2][\mathrm{Smad4}], \tag{30}$$

$$\frac{d[\mathrm{TF}]}{dt} = k_{10}[(\mathrm{PSmad2})_2][\mathrm{Smad4}] - k_{11}[\mathrm{TF}] - k_{12}[\mathrm{TF}][\mathrm{G_N}] + k_{-12}[\mathrm{A_N}], \tag{31}$$

$$\frac{d[\mathrm{A_N}]}{dt} = k_{12}[\mathrm{G_N}][\mathrm{TF}] - k_{-12}[\mathrm{A_N}]. \tag{32}$$

Applying the law of mass action, it is easy to show that

$$\frac{d[\mathrm{R}]}{dt} + \frac{d[\mathrm{R_A}]}{dt} + \frac{d[\mathrm{R_A S_2}]}{dt} = 0$$

in the core model studied here. Accordingly, there is a conserved quantity R_T, the total concentration of receptor,

$$R_T = [\mathrm{R}] + [\mathrm{R_A}] + [\mathrm{R_A S_2}],$$

from which [R] can be calculated given $[\mathrm{R_A}]$ and $[\mathrm{R_A S_2}]$. Proceeding similarly, we obtain the set of algebraic equations

$$[\mathrm{R}] = R_T - [\mathrm{R_A}] - [\mathrm{R_A S_2}], \tag{33}$$

$$[\mathrm{Smad2}] = S_2 - [\mathrm{R_A S_2}] - [\mathrm{PSmad2}] - 2[(\mathrm{PSmad2})_2] - 2[\mathrm{TF}] - 2[\mathrm{A_N}], \tag{34}$$

$$[\mathrm{Smad4}] = S_4 - [\mathrm{TF}] - [\mathrm{A_N}], \tag{35}$$

$$[\mathrm{G_N}] = G_{NT} - [\mathrm{A_N}], \tag{36}$$

respectively from the conservation relationships for the receptor, Smad2 (S_2 = total concentration of Smad2), Smad4 (S_4 = total concentration of Smad4) and *nodal* gene dosage (G_{NT}, the total concentration of the *nodal* gene). These algebraic equations close the system of equations (26) to (32).

The system of equations (26) to (32) always has the trivial steady state $[\mathrm{N_e}] = [\mathrm{R_A}] = [\mathrm{R_A S_2}] = [\mathrm{PSmad2}] = [(\mathrm{PSmad2})_2] = [\mathrm{TF}] = [\mathrm{A_N}] = 0$, as can easily be verified by substitution into the rate equations. All the coefficients of the characteristic polynomial evaluated at this steady state (not shown) are positive. Accordingly, this polynomial cannot have positive real roots (Briggs, 1985). Moreover, because this steady state is on the boundary of the physically realizable part of phase space, there cannot be oscillations around this steady state, i.e. the eigenvalues must be real. It follows that this steady state is stable.

To our knowledge, none of the parameters required in this model are available in the literature. Accordingly, we treated all of our parameters as

dimensionless quantities, and focused our efforts on demonstrating that the model has the capacity to display various behaviors, in particular bistability. By numerical experimentation, it is easy to find values of the rate constants displaying bistability, i.e. the appearance of a nontrivial stable steady state alongside the trivial steady state. We were somewhat aided in this search by our work with a previous, much simpler model (Ghimire and Roussel, unpublished notes), which suggested a parameter regime that might display bistability. Moreover, the graphical analysis discussed below also suggested some key parameters whose values might be particularly important, as explained later in this section.

Figure 2 shows a bifurcation diagram, in this case depicting the steady states of the model as functions of k_5. Note that there are two stable steady states (i.e. bistability) over the range $0 \leq k_5 \lesssim 2.072$, namely the zero steady state, corresponding to the right-hand developmental fate, and a high-Nodal state corresponding to the left-hand fate. The upper stable and unstable branches meet at a saddle-node bifurcation near $k_5 = 2.072$. For k_5 larger than the saddle-node bifurcation value, only the trivial steady state survives. We also observe (in the inset of Fig. 2) a transcritical bifurcation at $k_5 = 0$. Values of $k_5 < 0$ are of course physically meaningless, but it is very difficult to differentiate saddle-node and transcritical bifurcations without looking at what happens to either side of the bifurcation. Here we see that the unstable branch of steady states approaching from the right just touches the trivial steady state at $k_5 = 0$. For $k_5 < 0$, the trivial steady state becomes unstable while the other steady state becomes stable. An exchange of stability is characteristic of a transcritical bifurcation, although this one is unusual in that the two branches of steady states are only tangent at $k_5 = 0$ and do not cross each other.

There are two pathways for returning PSmad2 to its unphosphorylated state, one by direct dephosphorylation of PSmad2 [reaction (5)], and one by the action of the nuclear phosphatase that results in dissociation of the transcription factor complex and re-export of Smad2 and Smad4 to the cytoplasm, represented by the overall reaction (11). The latter is a simplified version of the known recycling pathway for Smad proteins (Schmierer et al., 2008), and is moreover required to conserve Smad2 and Smad4. Could we, however, drop reaction (5)? As it turns out, the answer is no. The characteristic polynomial at the trivial steady state (not shown) has a factor $(\lambda + k_5)$, leading to an eigenvalue of $-k_5$. If we eliminate reaction (5), i.e. set $k_5 = 0$, the characteristic polynomial evaluated at the trivial steady state then has

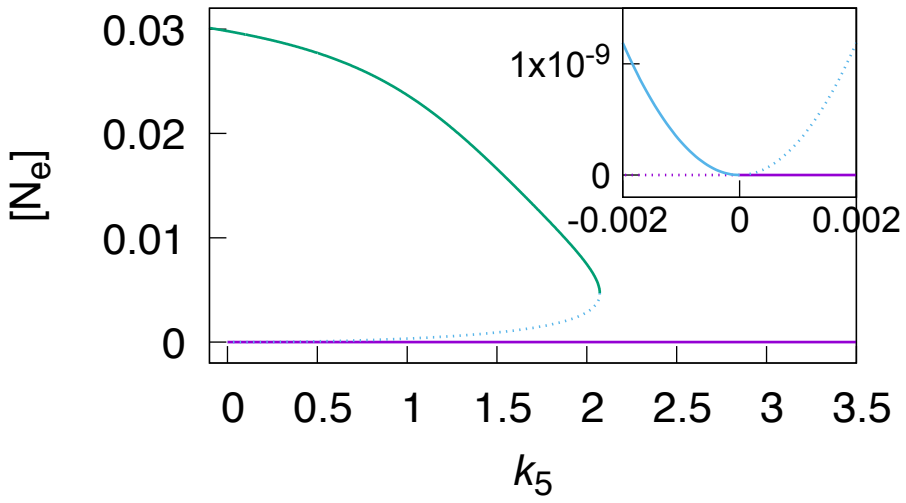

Figure 2: Effect of k_5 on the steady states of the core bistable Nodal model. The bifurcation diagram in the main panel was computed using XPPAUT (Ermentrout, 2002) as an interface to AUTO. All other bifurcation diagrams in this paper were computed using XPPAUT unless otherwise noted. The inset, which magnifies the region near $k_5 = 0$, was computed using the symbolic algebra system Maple. Solid lines represent stable steady states while dotted lines represent unstable steady states. Colors are used to distinguish branches of steady states, with corresponding branches colored identically in the two panels. Parameter values: $k_1 = 1$, $k_{-1} = 1$, $k_3 = 10$, $k_4 = 1$, $k_9 = 0.4$, $k_{10} = 0.1$, $k_{11} = 1$, $k_{12} = 10$, $k_{-12} = 10$, $k_{13} = 40$, $k_{18} = 1$, $S_2 = 15$, $S_4 = 0.2$, $R_T = 1$ and $G_{NT} = 0.01$.

a zero eigenvalue, which is related to the transcritical bifurcation mentioned above. A steady state with a zero eigenvalue automatically makes the system structurally unstable (Andronov and Pontrjagin, 1937). In the context of this specific model, we find, by numerical integration from initial conditions near the trivial steady state, that the latter is unstable at $k_5 = 0$, with all trajectories started from its vicinity ending up at the high-Nodal steady state (results not shown). Thus we have an unstable trivial steady state for $k_5 = 0$, but this same steady state is stable for any $k_5 > 0$, no matter how small. A model without reaction (5) is therefore structurally unstable with respect to this reaction.

4.2. Dimerization of PSmad2 and bistability

While all the reactions in the model are based on experimental observations, we have left out some relevant biochemistry for simplicity, such as the involvement of FoxH1 in the transcription factor (Iratni et al., 2002). It may then be asked whether the details we did include are strictly necessary. For example, our (simplified) transcription factor consists of two equivalents of PSmad2 and one of Smad4. Can we eliminate either the Smad2 dimerization or the subsequent binding to Smad4 and still get bistability? To study the role of PSmad2 dimerization, we replace reactions (9) to (11) by

$$\nu\,\mathrm{PSmad2} \xrightarrow{k'_9} \mathrm{C}_\nu, \tag{37}$$

$$\mathrm{C}_\nu + \mathrm{Smad4} \xrightarrow{k'_{10}} \mathrm{TF}, \tag{38}$$

$$\mathrm{TF} \xrightarrow{k'_{11}} \nu\,\mathrm{Smad2} + \mathrm{Smad4}, \tag{39}$$

where ν is a stoichiometric coefficient. If $\nu = 2$, we recover our original model; note that C_2 is just $(\mathrm{PSmad2})_2$. Fractional values of ν have no direct molecular interpretation, but we are interested in approaching $\nu = 1$, which corresponds to formation of a heterodimer of PSmad2 and Smad4, give or take the insertion of an extra step (conversion of PSmad2 to C_1) compared to direct heterodimerization. Nevertheless, we should be able to determine the dynamical consequence of smoothly varying the stoichiometry of the transcription factor through this model variation.

Replacing reactions (9) to (11) by (37) to (39) results in the replacement of Eqs. (29) to (31) by the following:

$$\frac{d[\mathrm{PSmad2}]}{dt} = k_4[\mathrm{R_A S_2}] - k_5[\mathrm{PSmad2}] - \nu k'_9[\mathrm{PSmad2}]^\nu, \tag{40}$$

$$\frac{d[\mathrm{C}_\nu]}{dt} = k'_9[\mathrm{PSmad2}]^\nu - k'_{10}[\mathrm{C}_\nu][\mathrm{Smad4}], \tag{41}$$

$$\frac{d[\mathrm{TF}]}{dt} = k'_{10}[\mathrm{C}_\nu][\mathrm{Smad4}] - k'_{11}[\mathrm{TF}] - k_{12}[\mathrm{TF}][\mathrm{G_N}] + k_{-12}[\mathrm{A_N}]. \tag{42}$$

Moreover, the conservation relation (34) is modified as follows:

$$[\mathrm{Smad2}] = S_2 - [\mathrm{R_A S_2}] - [\mathrm{PSmad2}] - \nu[\mathrm{C}_\nu] - \nu[\mathrm{TF}] - \nu[\mathrm{A_N}]. \tag{43}$$

For this model variation, the rank of the stoichiometric matrix $r = 7$ since there are 11 concentrations, and four conservation relations. We can work out the characteristic polynomial for the model with variable ν. For $\nu > 1$, all of the coefficients of the characteristic polynomial (not shown) are positive at the trivial steady state, which is therefore unconditionally stable for positive values of the parameters. However, for $\nu = 1$, the constant term of the characteristic polynomial evaluated at the trivial steady state becomes

$$c_7 = k_4 k'_{10} S_4 \left[k_{-1} k'_{11} k_{-12} k_{18} \left(k_5 + k'_9\right) - k_1 k_3 k'_9 k_{12} k_{13} G_{NT} R_T S_2\right]. \tag{44}$$

This coefficient may pass through zero. However, the transversality condition of the saddle-node bifurcation (Guckenheimer and Holmes, 1990, Theorem 3.4.1) is not satisfied, and the saddle-node bifurcation degenerates to a transcritical bifurcation. To illustrate this scenario, we need to generate bifurcation diagrams for different values of ν, ideally using a parameter that the cell could modulate. There are several such parameters in Eq. (44): additional transcription factors not considered in this model could modulate the rate of binding of the transcription factor to the promoter (k_{12}); the mean rate of gene expression from an active promoter (k_{13}) could likewise be modulated by a number of cellular control mechanisms; the availability of active phosphatases would affect both the decay of PSmad2 (k_5) and the dissociation of the transcription factor (k_{11}, k'_{11}); modulating the rate of protein decay (k_{18}) is a common control mechanism for cellular processes (Ciechanover et al., 2000); the display of receptors on the cell surface (R_T) can be controlled at a number of levels, from transcription to exocytosis; and the cellular level of Smad2 (S_2) could also differ in cells executing different developmental programs. We arbitrarily choose to vary R_T.

Figure 3 shows the transition from saddle-node bifurcations of the upper (stable) and middle (unstable) steady states to a transcritical bifurcation as $\nu \to 1$. The saddle-node bifurcation becomes an increasingly sharp corner as

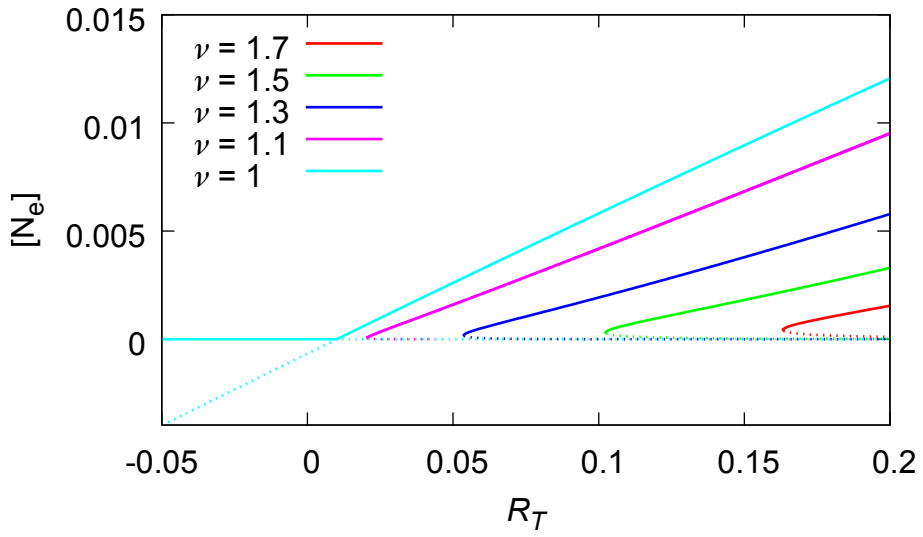

Figure 3: Transition from saddle-node bifurcations for $\nu > 1$ to a transcritical bifurcation at $\nu = 1$. Note that for $\nu > 1$, the trivial ($[\mathrm{N_e}] = 0$) solution is always stable for positive R_T, and is not plotted here for clarity, so that there are two stable steady states to the right of the saddle-node bifurcation, the trivial steady state being the only stable steady state to the left of the bifurcation. For $\nu = 1$ on the other hand, there is only one stable steady state at any value of R_T. For this figure, $k_1 = 10$, $k_{-1} = 1$, $k_3 = 10$, $k_4 = 1$, $k_5 = 2$, $k'_9 = 0.4$, $k'_{10} = 0.1$, $k'_{11} = 1$, $k_{12} = 10$, $k_{-12} = 10$, $k_{13} = 40$, $k_{18} = 1$, $S_2 = 15$, $S_4 = 0.2$ and $G_{NT} = 0.01$.

$\nu \to 1$. For $\nu = 1$, there are only two steady states, namely the trivial steady state and a single "high-Nodal" state. For the parameters of this figure, the transcritical bifurcation for $\nu = 1$ occurs at $R_T = 0.01$, as calculated by setting c_7 from Eq. (44) equal to zero. Note that the replacement of the saddle-node bifurcation by a transcritical bifurcation means that bistability cannot be obtained in this model without the formation of PSmad2 dimers.

There is a single critical fragment of order 7, with characteristic value $K_{S_7} = -\nu$, illustrated in Fig. 4. Note the correspondence between the reactions in the critical fragment and the rate constants in the negative term in Eq. (44). In order for the constant term in the characteristic polynomial to pass through zero, which is required for the saddle-node bifurcation that generates bistability, this negative term must be sufficiently large. The structure of the critical fragment informed us, at an early stage of this project, about the rate constants whose values, if made larger, might favor bistabil-

ity. This includes both the rate constants in the critical fragment itself, and those rate constants that tended to make the concentrations of the species in this fragment larger. Thus, the identification of critical fragments not only identifies the mechanistic features responsible for (in this case) bistability, but also directs the search of parameter space.

Note that $K_{S_7} < 0$ for any positive ν, including $\nu = 1$. This leads to an interesting observation not heretofore discussed in the literature to our knowledge: A critical fragment of order r indicates the potential for a negative term in the constant term of the characteristic polynomial (c_r), and therefore the potential for that term to pass through zero. However, the saddle-node is not the only type of bifurcation associated with $c_r = 0$; both transcritical and pitchfork bifurcations can also occur when this coefficient becomes zero, the latter two being degenerate forms of the saddle-node bifurcation (Guckenheimer and Holmes, 1990, section 3.4). Accordingly, a critical fragment is a necessary (but not sufficient) condition for any of the three bifurcations in this class, saddle-node, transcritical, or pitchfork.

4.3. Saturability and bistability

Each of the components in this model subject to a conservation law could potentially be saturated. The question then arises whether saturation of certain components (enzymes, transcription factors, gene promoter) is important to the bistable network.

We can study whether Michaelis-Menten kinetics in the phosphorylation of Smad2 is important by replacing reactions (3) and (4) by

$$\mathrm{R_A} + \mathrm{Smad2} \xrightarrow{k_3'} \mathrm{R_A} + \mathrm{PSmad2}. \tag{45}$$

Other reactions are as in the core model, including the formation of the PSmad2 dimer. Eliminating the saturable kinetics of $\mathrm{R_A}$ reduces the rank of the model to 6. The model retains one critical fragment of order 6 with $K_{S_6} = -2$, illustrated in Fig. 5. Thus, the network is still compatible with bistability, and we have confirmed numerically that bistability is observed with this simplification (results not shown).

Looking at Eqs. (23) to (25), we see that the key factors that determine whether or not a fragment will be critical are any stoichiometric coefficients greater than 1, the number of cycles in a fragment, and whether these cycles contain an odd or even number of negative paths. If a model has a critical fragment, then model simplifications that preserve these attributes will retain

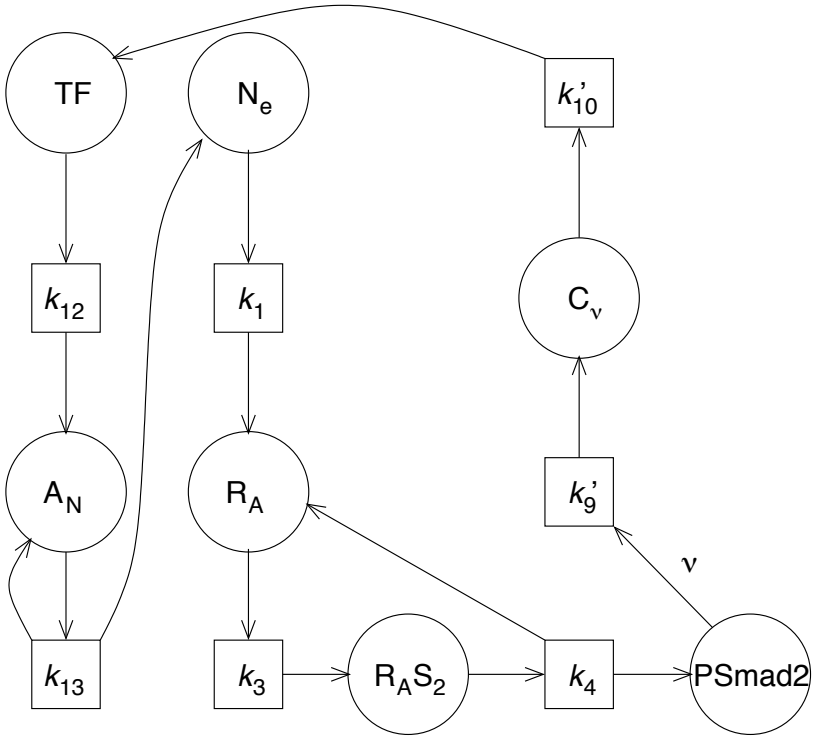

Figure 4: Critical fragment for the model with variable PSmad2 stoichiometry [Eqs. (26) to (28), (32), (33), (35), (36) and (40) to (43)]. Reactions are labeled by the corresponding rate constant. The edges are weighted by the corresponding stoichiometric coefficients, typically 1 and not explicitly noted, with the exception of the PSmad2 $\to k_9'$ edge, which has weight ν.

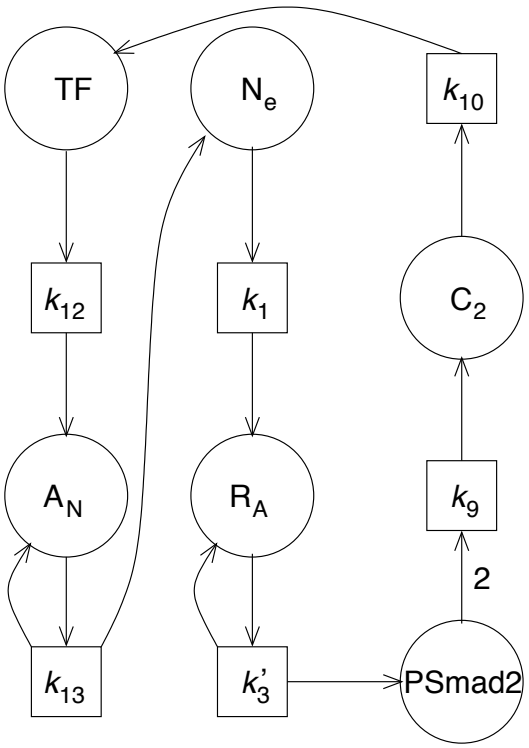

Figure 5: Critical fragment for the model in which saturable phosphorylation of Smad2 has been replaced by the bimolecular approximation (45). Note that we use C_2 as a shorthand for $(\text{PSmad2})_2$.

a critical fragment. The graphical analysis therefore directly suggests model simplifications, notably the shortening of cycles. The graphical analysis can also be used to determine that some model additions would *not* compromise model behavior, in this case bistability.

Examining Figs. 4 and 5, we see that the structure of the critical fragment is unaffected by binding to Smad4 (reactions associated with k_{10} or k'_{10}). We could thus remove the corresponding reaction and intermediate, i.e. have $(\text{PSmad2})_2$ function as the transcription factor directly. Conversely, we could add in binding of the $(\text{PSmad2})_2 \cdot \text{Smad4}$ heterotrimer to FoxH1 to form the active transcription factor without changing the structure of the critical fragment. From these observations and our prior observations on the stoichiometry with respect to PSmad2, it follows that the key source of nonlinearity for bistability is the formation of the PSmad2 dimer, and not saturable binding to additional factors (Smad4, FoxH1) in forming the transcription factor.

There remains to examine saturability at the gene promoter as a potentially important nonlinearity. We can deal with this analogously to the saturability of the kinase R_A by replacing Eqs. (12) and (13) by

$$\text{TF} \xrightarrow{k'_{13}} \text{TF} + \text{N}_\text{e}. \tag{46}$$

If we do this, we again maintain bistability, but numerically we find that the basin of attraction of the trivial steady state becomes very small in the parameter range we have been considering (results not shown). This is not surprising given the linear increase in the rate of synthesis of Nodal with [TF] in (46). We can compensate by decreasing k'_{13}, but it is clear that saturable binding to the promoter is important from a quantitative perspective, even if it is qualitatively dispensable.

Taking all of these results together, we find that in this particular model, saturability turns out not to be a key issue for bistability, although it may be important for determining the basins of attraction of the two stable steady states.

5. The complete Nodal-Lefty model

We now turn to the complete Nodal-Lefty model described in section 2. As seen above, the Nodal subsystem is, of itself, capable of bistability. From the point of view of allowing for left (high Nodal) and right (low Nodal)

cell states, Lefty is therefore unnecessary. Lefty might play a role in the spatio-temporal development of the Nodal distribution, as suggested by Turing (Nakamura et al., 2006) and wave-propagation failure models (Middleton et al., 2013). Another possibility, suggested by the recent experiments of Rogers et al. (2017), is that Lefty modulates the expression of Nodal, but doesn't have a specific role in pattern formation. We will leave a study of the spatio-temporal behavior of this model to a later paper and focus here on understanding the cell-autonomous response of the model to Nodal and Lefty.

5.1. Rate equations

The following rate equations are obtained by applying the law of mass action to the reactions presented in section 2:

$$\begin{aligned}\frac{d[\mathrm{N_e}]}{dt} &= -k_1[\mathrm{N_e}][\mathrm{R}] + k_{-1}[\mathrm{R_A}] - k_6[\mathrm{N_e}] + k_{-6}[\mathrm{N_i}] \\ &\quad + k_{13}[\mathrm{A_N}] + k_{14}[\mathrm{G_N}] - k_{18}[\mathrm{N_e}],\end{aligned} \tag{47}$$

$$\frac{d[\mathrm{N_i}]}{dt} = k_6[\mathrm{N_e}] - k_{-6}[\mathrm{N_i}] - k_{20}[\mathrm{N_i}], \tag{48}$$

$$\begin{aligned}\frac{d[\mathrm{L_e}]}{dt} &= -k_2[\mathrm{L_e}][\mathrm{R}] + k_{-2}[\mathrm{R_X}] - k_7[\mathrm{L_e}] + k_{-7}[\mathrm{L_i}] \\ &\quad + k_{16}[\mathrm{A_L}] + k_{17}[\mathrm{G_L}] - k_{19}[\mathrm{L_e}],\end{aligned} \tag{49}$$

$$\frac{d[\mathrm{L_i}]}{dt} = k_7[\mathrm{L_e}] - k_{-7}[\mathrm{L_i}] - k_8[\mathrm{R_A}][\mathrm{L_i}] + k_{-8}[\mathrm{R_L}] - k_{21}[\mathrm{L_i}], \tag{50}$$

$$\begin{aligned}\frac{d[\mathrm{R_A}]}{dt} &= k_1[\mathrm{R}][\mathrm{N_e}] - k_{-1}[\mathrm{R_A}] - k_3[\mathrm{R_A}][\mathrm{Smad2}] \\ &\quad + (k_{-3} + k_4)[\mathrm{R_A S_2}] - k_8[\mathrm{R_A}][\mathrm{L_i}] + k_{-8}[\mathrm{R_L}],\end{aligned} \tag{51}$$

$$\frac{d[\mathrm{R_A S_2}]}{dt} = k_3[\mathrm{R_A}][\mathrm{Smad2}] - (k_{-3} + k_4)[\mathrm{R_A S_2}], \tag{52}$$

$$\frac{d[\mathrm{R_X}]}{dt} = k_2[\mathrm{L_e}][\mathrm{R}] - k_{-2}\mathrm{R_X}, \tag{53}$$

$$\frac{d[\mathrm{R_L}]}{dt} = k_8[\mathrm{R_A}][\mathrm{L_i}] - k_{-8}[\mathrm{R_L}], \tag{54}$$

$$\begin{aligned}\frac{d[\mathrm{PSmad2}]}{dt} &= k_4[\mathrm{R_A S_2}] - k_5[\mathrm{PSmad2}] \\ &\quad - 2k_9[\mathrm{PSmad2}]^2 + 2k_{-9}[(\mathrm{PSmad2})_2],\end{aligned} \tag{55}$$

$$\frac{d[(\mathrm{PSmad2})_2]}{dt} = k_9[\mathrm{PSmad2}]^2 - k_{-9}[(\mathrm{PSmad2})_2] - k_{10}[(\mathrm{PSmad2})_2][\mathrm{Smad4}], \tag{56}$$

$$\frac{d[\mathrm{TF}]}{dt} = k_{10}[(\mathrm{PSmad2})_2][\mathrm{Smad4}] - k_{11}[\mathrm{TF}] - k_{12}[\mathrm{TF}][\mathrm{G_N}] + k_{-12}[\mathrm{A_N}] - k_{15}[\mathrm{TF}][\mathrm{G_L}] + k_{-15}[\mathrm{A_L}], \tag{57}$$

$$\frac{d[\mathrm{A_N}]}{dt} = k_{12}[\mathrm{G_N}][\mathrm{TF}] - k_{-12}[\mathrm{A_N}], \tag{58}$$

$$\frac{d[\mathrm{A_L}]}{dt} = k_{15}[\mathrm{G_L}][\mathrm{TF}] - k_{-15}[\mathrm{A_L}]. \tag{59}$$

The following conservation relations are easily shown to arise from the mechanism:

$$R_T = [\mathrm{R}] + [\mathrm{R_A}] + [\mathrm{R_A S_2}] + [\mathrm{R_X}] + [\mathrm{R_L}], \tag{60}$$

$$S_2 = [\mathrm{Smad2}] + [\mathrm{R_A S_2}] + [\mathrm{PSmad2}] + 2[(\mathrm{PSmad2})_2] + 2[\mathrm{TF}] + 2[\mathrm{A_N}] + 2[\mathrm{A_L}], \tag{61}$$

$$S_4 = [\mathrm{Smad4}] + [\mathrm{TF}] + [\mathrm{A_N}] + [\mathrm{A_L}], \tag{62}$$

$$G_{NT} = [\mathrm{G_N}] + [\mathrm{A_N}], \tag{63}$$

$$G_{LT} = [\mathrm{G_L}] + [\mathrm{A_L}]. \tag{64}$$

In these equations, R_T is the total receptor concentration, S_2 is the total Smad2 concentration, S_4 is the total Smad4 concentration, G_{NT} is the *nodal* gene dosage, and G_{LT} is the *lefty* gene dosage. These equations are used, respectively, to calculate the concentrations of Smad2, Smad4, R, $\mathrm{G_N}$ and $\mathrm{G_L}$ needed to close the system of equations (47) to (59).

5.2. Stability and basin of attraction of the low-Nodal steady state

As for the core bistable model, the full set of differential equations has a trivial (zero) steady state when leaky gene expression is excluded, i.e. when $k_{14} = k_{17} = 0$. We can evaluate the characteristic polynomial at the trivial steady state (not shown), and we find that all of the coefficients of this polynomial are positive. Thus, the trivial steady state is always stable, just as it was in the core bistable model. Also as in the core bistable model, the characteristic polynomial in the absence of leaky gene expression has a factor of $(\lambda + k_5)$, so the direct dephosphorylation of PSmad2 [reaction (5)] is essential in the full model as well.

In order to gauge the importance of Lefty in the cell-autonomous dynamics, we considered the response of a cell to the initial extracellular Nodal and Lefty concentrations starting from initial conditions where all the other variables were set to zero. This is intended to mimic an *in vitro* experiment in which a cell culture (possibly a cell suspension) initially near the low-Nodal steady state is injected with some mixture of Nodal and Lefty at $t = 0$. It is not intended to directly model the situation in an embryo, in which cell-cell communication via extracellular Nodal and Lefty is important. These numerical experiments should nevertheless give an indication of the sensitivity of cells to the extracellular Nodal and Lefty concentrations, even if the diagrams do not directly reflect the behavior of the cells in a tissue. The differential equations were integrated using the Matlab stiff integrator ODE15S until a steady state was reached. By golden-section search, we located the boundary between the two basins of attraction in the plane of initial N_e and L_e concentrations. The sensitivity of the results to the numerical tolerances was verified and found to be negligible. Figure 6 shows these basins for the parameters of Table 2. Even at zero initial $[L_e]$, it takes quite a large initial Nodal concentration to push the cells to the high-Nodal steady state. For perspective, the steady-state value of $[N_e]$ in the high-Nodal state is 0.025 at these parameters, about tenfold lower than the concentration of Nodal required to converge to the high steady-state. The value of $[N_e]_0$ required to reach the high-Nodal steady state is very sensitive to the value of k_1. Doubling this value substantially decreases the threshold, and makes the system much less sensitive to the initial Lefty concentration (Fig. 7).

We included reactions (14) and (17) to verify the robustness of the model results to leaky gene expression. To study this issue, we varied the values of k_{14} and k_{17} independently, each from 10^{-5} to 10^{0}. When we increase k_{14}, the rate constant for leaky gene expression from the *nodal* gene, the Nodal concentrations increase in both stable steady states, but decrease in the unstable steady state (Fig. 8). Consequently, there is a saddle-node bifurcation involving the low-Nodal branch near $k_{14} = 9.90 \times 10^{-3}$, with only the high-Nodal steady state surviving for larger values of k_{14}. The value of k_{14} at the saddle-node point represents a small leak, but not an insignificant one, corresponding to approximately 0.05% of the value of k_{13}, the rate constant associated with *nodal* expression under the control of the transcription factor [reaction (13)]. At least for the parameters studied here, the ability of the Nodal-Lefty system to generate two stable steady states therefore depends on the Nodal gene promoter being stringently controlled by its transcription

Table 2: Default parameter values used in this study

Parameter	Value	Parameter	Value
Ligand-receptor kinetics		*Transcriptional control*	
k_1	0.1	k_9	1.0
k_{-1}	0.24	k_{-9}	8.0
k_2	2.0	k_{10}	1.0
k_{-2}	0.1	k_{11}	0.1
k_3	1.0	k_{12}	1.0
k_{-3}	1.0	k_{-12}	1.0
k_4	0.1	k_{13}	20.0
k_{-4}	0.1	k_{14}	1.0×10^{-5}
k_5	0.1	k_{15}	1.0
k_6	0.1	k_{-15}	1.0
k_{-6}	0.1	k_{16}	15.0
k_7	0.1	k_{17}	1.0×10^{-5}
k_{-7}	0.1		
k_8	1.0	*Conserved quantities*	
k_{-8}	0.1	S_2	20.0
		S_4	10.0
Protein degradation		R_T	1.0
k_{18}	0.1	G_{NT}	0.01
k_{19}	0.1	G_{LT}	0.01
k_{20}	10.0		
k_{21}	10.0		

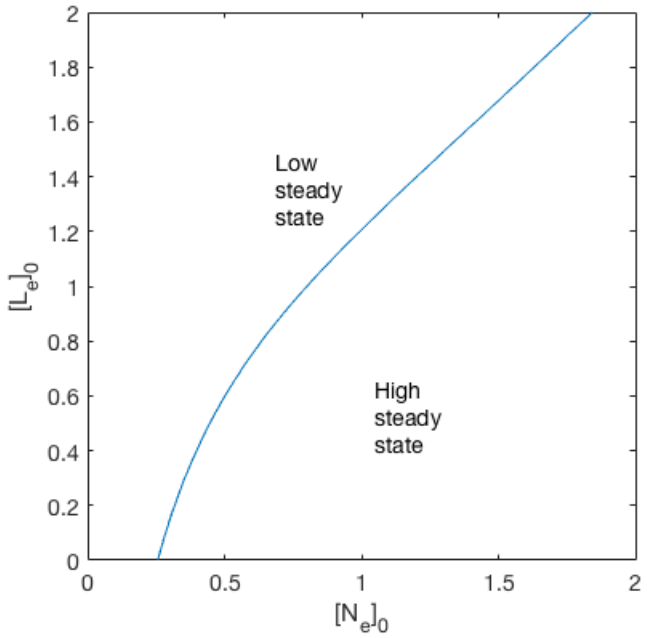

Figure 6: Basins of attraction of the two stable steady states in the space of initial Nodal and Lefty concentrations, all other initial concentrations being set to zero, using the parameters of Table 2.

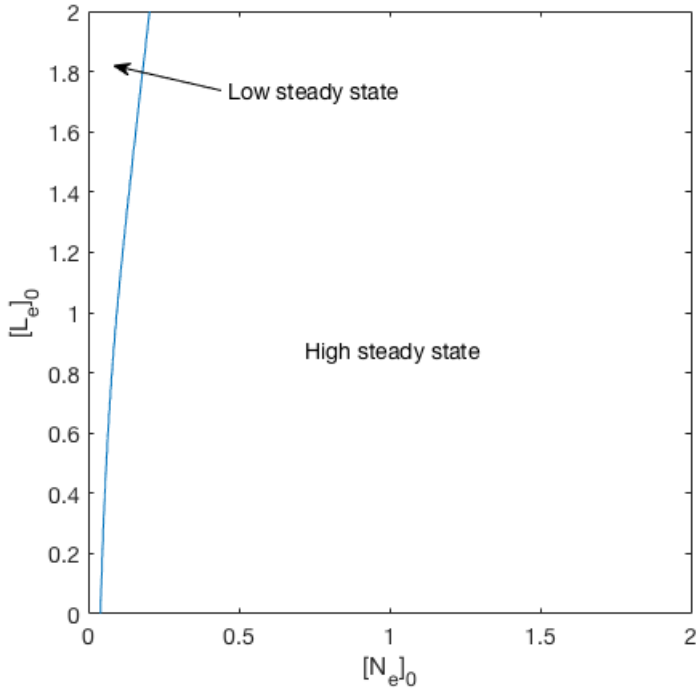

Figure 7: Basins of attraction of the two stable steady states in the space of initial Nodal and Lefty concentrations using the parameters of Table 2, except $k_1 = 0.2$.

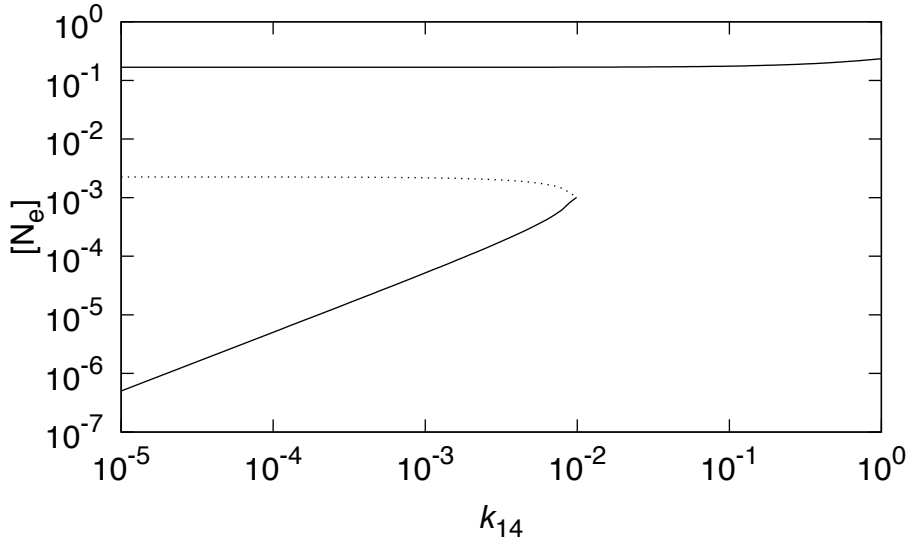

Figure 8: Bifurcation diagram varying k_{14}, with the other parameters set as in Table 2. This diagram was computed using the symbolic algebra system Maple.

factor.

Varying k_{17} eventually results in a saddle-node bifurcation that destroys the high-Nodal and unstable steady states (results not shown). The saddle-node bifurcation occurs at $k_{17} \approx 0.028$, or about 0.2% of k_{16}, the rate constant for *lefty* expression under the control of the transcription factor [reaction (16)]. Over a wide range of k_{17} values preceding this bifurcation, the Nodal concentration at the three steady states varies weakly. For example, from $k_{17} = 10^{-5}$ to 10^{-3}, a hundredfold increase in this rate constant, the Nodal concentration in the high-Nodal steady state decreases from 2.534×10^{-2} to 2.520×10^{-2}. The overall control system is therefore more robust to leaky expression of *lefty* than to leaky expression of *nodal*.

We now consider a mutant that has an intact signaling system, and is thus able to *respond* to externally provided Lefty, but that is unable to produce Lefty itself. Again note that our numerical experiment corresponds to delivering an initial bolus of Nodal and Lefty to the cells, and allowing them to evolve autonomously from that point on. The basins of attraction of the two steady states with respect to the initial external concentrations of Lefty and Nodal for this mutant are shown in Fig. 9. Comparing the mutant of Fig. 9 to the "wild type" of Fig. 6, we see that the behavior is

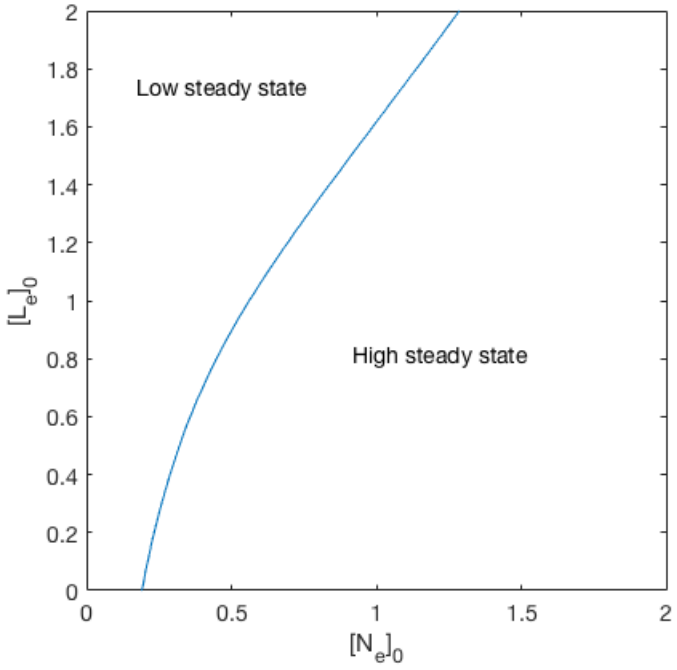

Figure 9: Basins of attraction of the two stable steady states in the space of initial Nodal and Lefty concentrations for a mutant that is unable to produce Lefty, but is otherwise intact. For this calculation, the parameters of Table 2 were used except for $k_{16} = k_{17} = 0$.

qualitatively the same. The Lefty knock-out mutant however requires a lower $[\mathrm{N_e}]_0$ to reach the high-Nodal steady state at any initial Lefty concentration, as might be expected given that it does not itself produce the inhibitor.

Another interesting mutant, particularly given the experimental study of Rogers et al. (2017) showing that co-control of *nodal* and *lefty* expression is dispensable for normal development, is one in which *lefty* is constitutively expressed. Our model includes mutants constitutively expressing *lefty* as a special case by setting $k_{15} = 0$. Reaction (17), which does not depend on the activation of the Lefty gene by the Nodal signaling pathway, then allows for constitutive expression of *lefty*. Figure 10 shows the behavior of such a mutant, varying the rate constant for constitutive expression. The system can tolerate moderately high levels of constitutive expression of *lefty* and still maintain bistability. Thus, as was found experimentally by Rogers et al. (2017), the possibility of maintaining two developmental domains, left and

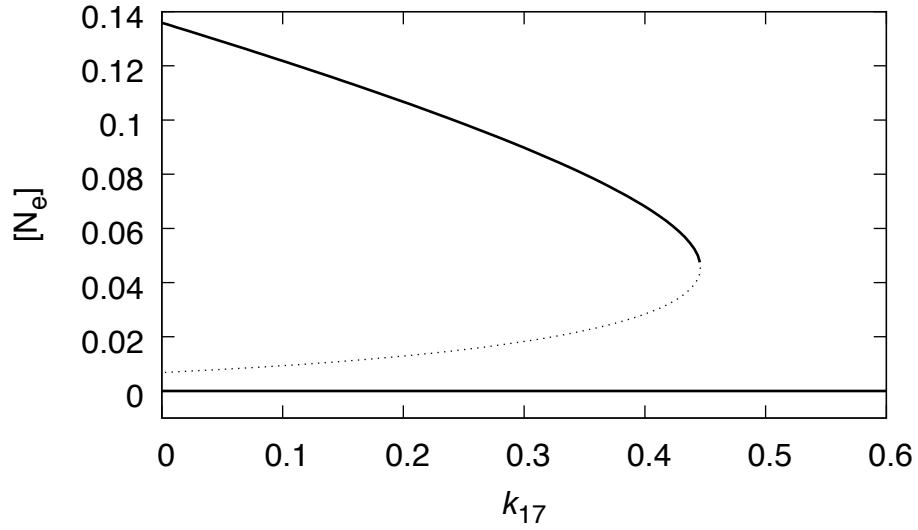

Figure 10: Bifurcation diagram for the study of a mutant constitutively expressing *lefty*. For this mutant, $k_{15} = 0$, turning off expression under the control of the inducible promoter, and other parameters are set as in Table 2. Varying k_{17} then corresponds to varying the rate of constitutive expression.

right, does not strictly depend on the control of *lefty* expression by Nodal, provided some other mechanism can set appropriate initial conditions for the Nodal subsystem. We offer some thoughts on this point in the discussion.

In developmental systems, we also have to allow for the possibility that the kinetic parameters are themselves variable in time or space, as gene expression is typically regulated by pathways whose activation changes with time or in different spatial contexts. For example, the binding of a transcription factor at a gene promoter could be modulated by epigenetic modification of histones or by the binding of other factors at or near the promoter, modifying the promoter's activity. A very detailed model could include such reactions explicitly. To get a sense of the effects of such modifications, we can also just vary the the rate constant for binding of a transcription factor to a promoter. (An argument could also be made for capturing these effects by varying the instantaneous gene dosage, e.g. G_{NT} or G_{LT} in this model.) For example, we could vary the rate constant for binding of the transcription factor in this model at the *lefty* promoter, k_{15}. Figure 11 shows the results of such a calculation. As might have been guessed, if induction of the *lefty* gene is too

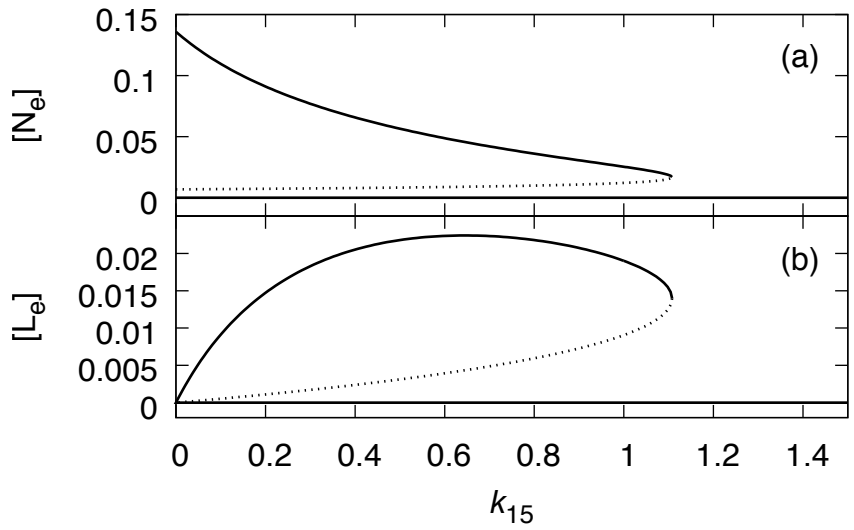

Figure 11: Bifurcation diagram with respect to k_{15}, the rate constant for binding of the transcription factor to the *lefty* promoter, for the parameters of Table 2. Both [N_e] [panel (a)] and [L_e] [panel (b)] as a function of the parameter are shown.

strong, a saddle-node bifurcation destroys the high-Nodal/high-Lefty steady state. Thus, epigenetic modifications or activators that favor transcription of *lefty* can shut down the Nodal signaling pathway. On the other hand, if Nodal is needed but not Lefty in some particular developmental context, inhibitory histone modifications or the binding of repressors to the promoter, either of which could be represented by a decreased value of k_{15}, will leave the bistability of the Nodal subsystem intact while shutting down expression of *lefty*.

5.3. Inhibition mechanisms compared

The competition between Nodal and Lefty to bind at the Nodal receptor is well known. The uncompetitive inhibition by intracellular Lefty on the other hand has only been reported in a single study, to our knowledge (Ulloa and Tabibzadeh, 2001). Assuming that the latter mode of inhibition does indeed operate in mice, what effect does it have compared to the competitive inhibition by L_e?

Our original parameters (Table 2) are ill-suited to study this question because competitive inhibition by extracellular Lefty dominates over the al-

Table 3: Inhibition-balanced parameter set. Only the parameters that differ from those given in Table 2 are shown here.

Parameter	Value
k_2	5
k_7	1.0
k_{-7}	1.0
k_8	250.0
k_{19}	1.5
k_{21}	0.1

ternative uncompetitive inhibition control mechanism. Thus, we developed a second set of parameters that is balanced in the following sense: First, the intracellular and extracellular Lefty concentrations in the high-Nodal steady state are similar (within 10% of each other). Second, the concentrations of the two inhibited complexes are also similar in the high-Nodal steady state. The differences between our default parameters and this "inhibition-balanced" parameter set are given in Table 3. These parameters allow us to compare the two inhibition channels on a roughly equal footing.

We use two different, complementary methods to study the dynamical effects of inhibition. In one set of calculations, we compute bifurcation diagrams with respect to k_{15}, the rate constant for binding of the transcription factor at the *lefty* promoter. This will modulate the overall amount of Lefty protein, and thus the importance of inhibition. In our second set of calculations, we compute basins of attraction for the two steady states as we did in the previous section. This will tell us how sensitive the final state is to the Lefty concentration.

Figure 12 shows the results of the two calculations described above for the parameters of Table 3. Qualitatively, these results are quite similar to those shown in Figs. 6 and 11. Thus, the new parameter set, while quite differently balanced than our previous set of parameters, does not change the behavior of the model in any significant way.

Figure 12 provides a baseline for a pair of numerical experiments in which we inactivate each of the inhibition pathways in turn. Fig. 13 shows the results of turning off the uncompetitive pathway by setting $k_8 = 0$. Although there are some quantitative differences between Figs. 12 and 13, the results are very similar. This suggests immediately that competitive inhibition by extracellular Lefty is more effective than uncompetitive inhibition by intra-

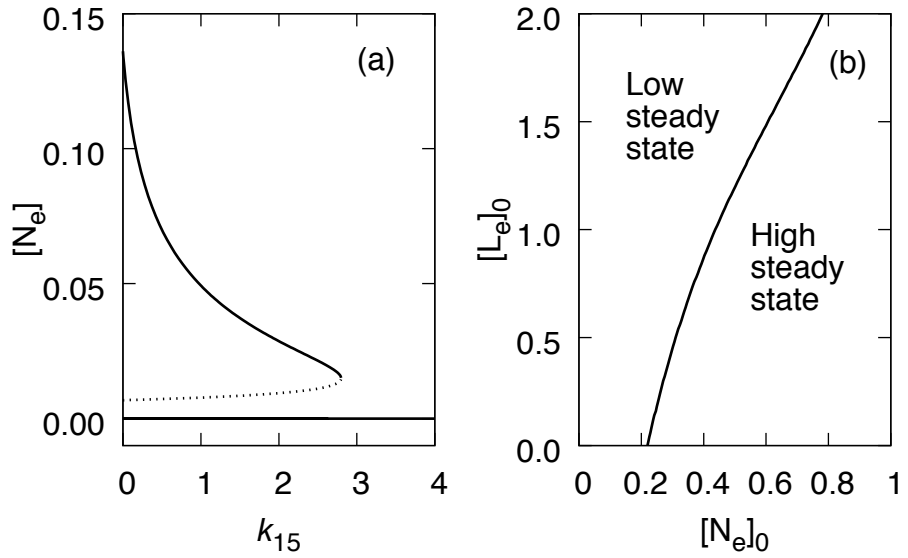

Figure 12: (a) Bifurcation diagram with respect to the rate constant for binding of the transcription factor to the *lefty* promoter, k_{15}, and (b) basins of attraction of the two stable steady states with respect to the initial extracellular Nodal and Lefty concentrations for the parameters of Table 3.

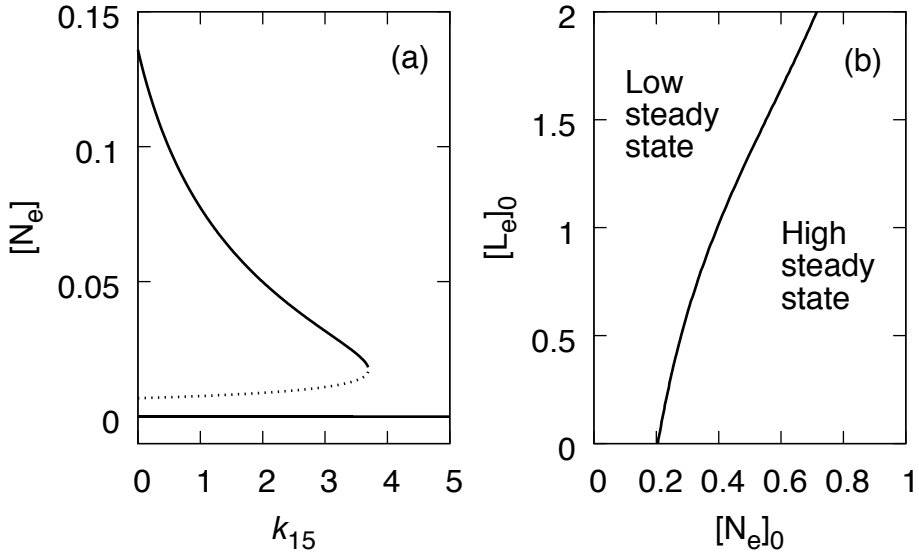

Figure 13: (a) Bifurcation diagram with respect to k_{15}, and (b) basins of attraction of the two stable steady states using the same parameters as in Fig. 12, except $k_8 = 0$, turning off the uncompetitive inhibition pathway involving internalized Lefty.

cellular Lefty.

This tentative conclusion is reinforced by looking at what happens when competitive inhibition is turned off ($k_2 = 0$) and only uncompetitive inhibition remains. Comparing Figs. 13(a) and 14(a), we see that a much larger value of k_{15} is required to reach the saddle-node bifurcation if only uncompetitive inhibition is active than if the system relies exclusively on competitive inhibition. More strikingly, the basin boundary becomes more nearly vertical in this case [Fig. 14(b)], indicating that the system is almost completely insensitive to Lefty in this regime. It is possible that there are parts of parameter space where uncompetitive inhibition is more effective, but our results to date suggest that uncompetitive inhibition, if it occurs at all, exerts very poor control over Nodal expression.

5.4. Other dynamical behaviors

The critical fragment of the minimal bistable (Nodal-only) model (Fig. 4 with $\nu = 2$) of course persists in the larger Nodal-Lefty model, where it is now a critical fragment or order $k < r$, r the rank of the full model. Thus the larger model meets a necessary condition for an Andronov-Hopf bifurcation

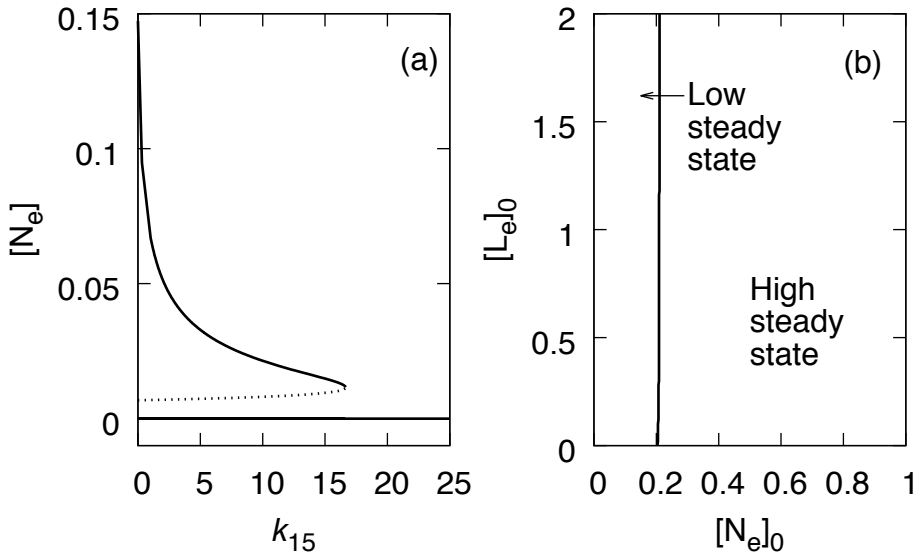

Figure 14: (a) Bifurcation diagram with respect to k_{15}, and (b) basins of attraction of the two stable steady states using the same parameters as in Fig. 12, except $k_2 = 0$, turning off competitive inhibition by extracellular Lefty.

(Mincheva and Roussel, 2007). We have in fact found two distinct Andronov-Hopf bifurcation scenarios, described below.

The first scenario is a conventional supercritical Andronov-Hopf bifurcation (Fig. 15). Limit cycles are observed only over a narrow range of k_2 values in this parameter regime, with the Andronov-Hopf bifurcation found near $k_2 = 857.34$, and the limit cycle suddenly disappearing near $k_2 = 863.37$ in a homoclinic bifurcation. (See Fig. 16 showing the characteristic divergence of the period as the bifurcation is approached.)

The oscillations observed in this regime are competitive binding oscillations (Ngo and Roussel, 1997), and can be understood with reference to Fig. 17. For the parameters where these oscillations are observed, binding of Lefty to the receptor is very strong, so the concentration of the complex R_X is large. Moreover, the receptor holds most of the Lefty protein at any given time. When $[R_A]$ is small, Lefty and Nodal are synthesized at a negligible rate. Slow release of Lefty from the receptor, and relatively slow degradation kinetics mean that the concentration of Lefty, and thus of R_X, decays slowly. Nodal decays more rapidly, but not so rapidly as to be completely depleted during a cycle. The concentration of R_X eventually drops sufficiently to allow

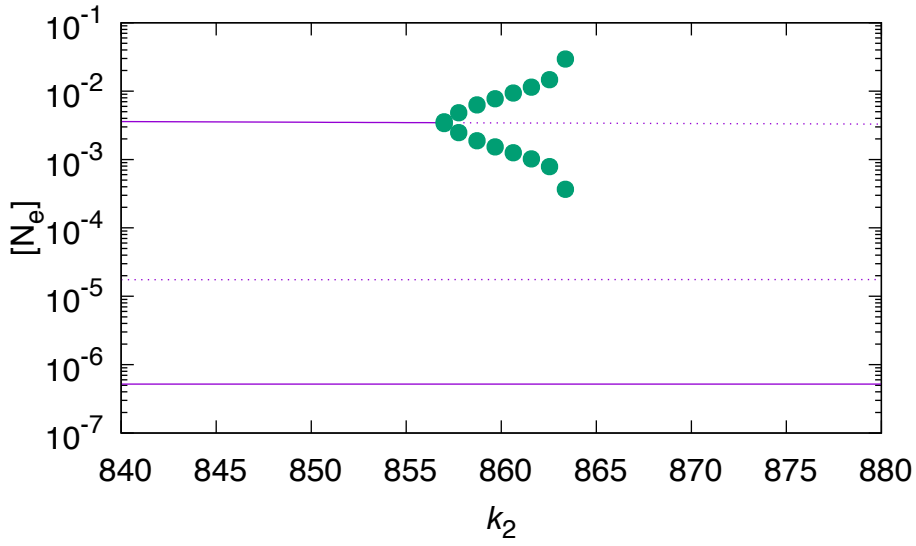

Figure 15: Bifurcation diagram obtained with the parameters of Table 2, with the following changes: $k_1 = 1$, $k_{12} = 2$. Solid curves represent stable steady states, dotted curves are unstable steady states, and filled circles are the minima and maxima of stable limit cycles. Note the logarithmic scale of the ordinate.

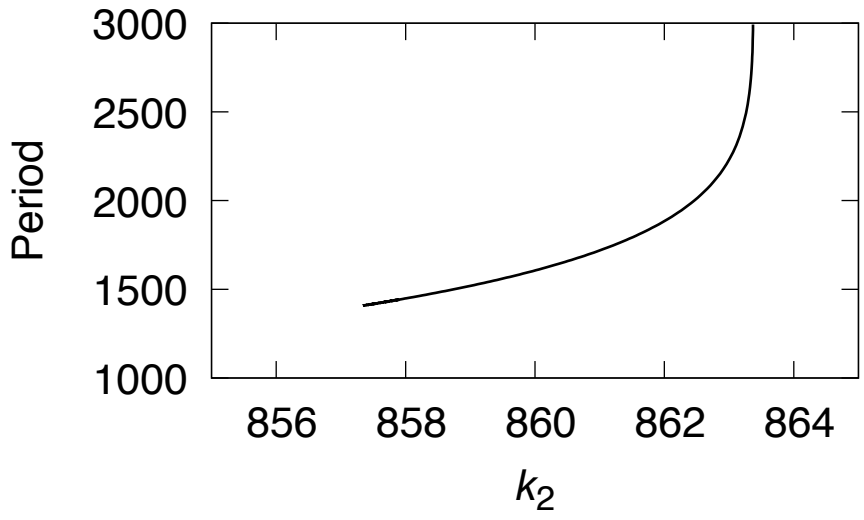

Figure 16: Frequency of the limit cycle over its range of existence corresponding to the bifurcation diagram of Fig. 15.

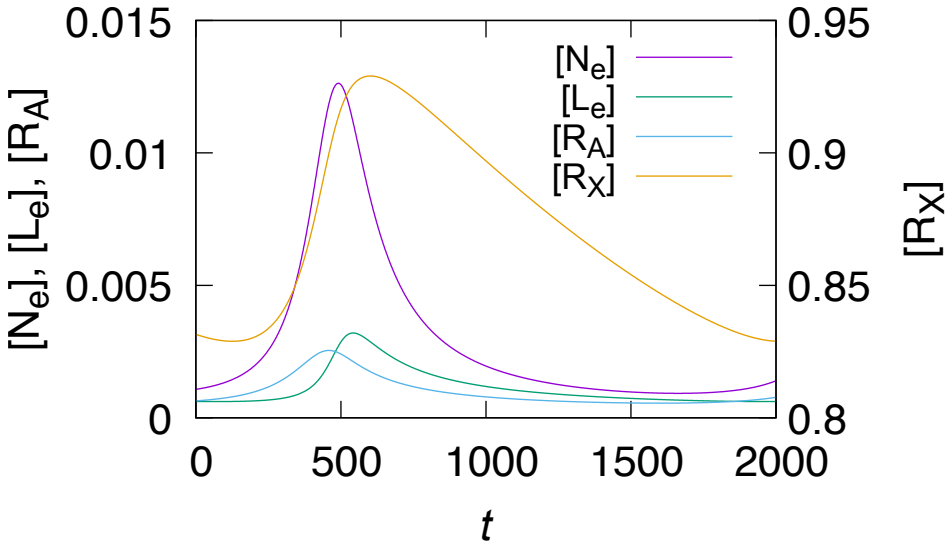

Figure 17: Key variables shown over one full cycle of oscillations for the parameters of Fig. 15, with $k_2 = 862$.

Nodal to bind to its receptor, leading to synthesis of Nodal and Lefty. The autocatalytic nature of the Nodal synthetic system causes a rapid increase in Nodal, and thus in $[R_A]$. Because of the high rate constant for binding of Lefty to the receptor, the synthesis pathway is however rapidly shut down, returning the system to the state dominated by decay of the Nodal and Lefty concentrations.

In the second scenario, a subcritical Andronov-Hopf bifurcation occurs near $k_2 = 20.059$ (Fig. 18). An unstable limit cycle emerges to the left of the bifurcation point. To the right of the bifurcation point, the upper branch of steady states loses stability. The upper and middle branches of steady states eventually annihilate in a saddle-node bifurcation near $k_2 = 22.354$.

The behavior near the subcritical Andronov-Hopf bifurcation is shown in a series of phase portraits shown in Fig. 19. For k_2 below the bifurcation (e.g. $k_2 = 19.1$ and 19.28), the unstable manifold of the saddle point consists of two heteroclinic orbits that respectively reach the low- and high-Nodal steady states, the latter being a stable focus at these parameters. Trajectories started from sufficiently large $[N_e]$ will typically loop around the basin of attraction of the stable focus, and terminate at the low-Nodal steady state. At $k_2 \approx 19.290$, a homoclinic bifurcation occurs, creating a closed orbit. For

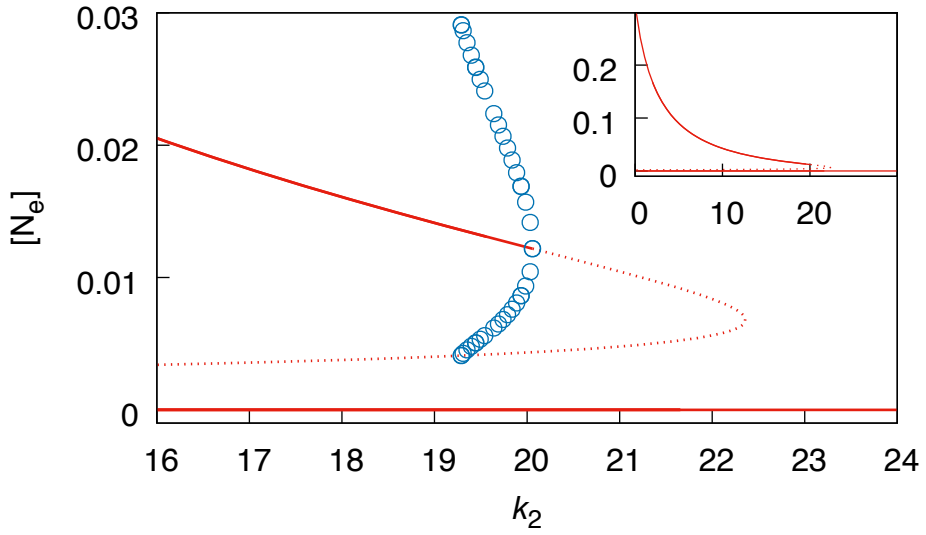

Figure 18: Bifurcation diagram varying k_2 with $k_{12} = 2$ and other parameters set as in Table 2. Solid lines represent stable steady states, dotted lines unstable steady states, and open circles the minimum and maximum values of unstable limit cycles. The inset shows the diagram over a wider range of k_2 values, with the unstable limit cycles omitted for clarity.

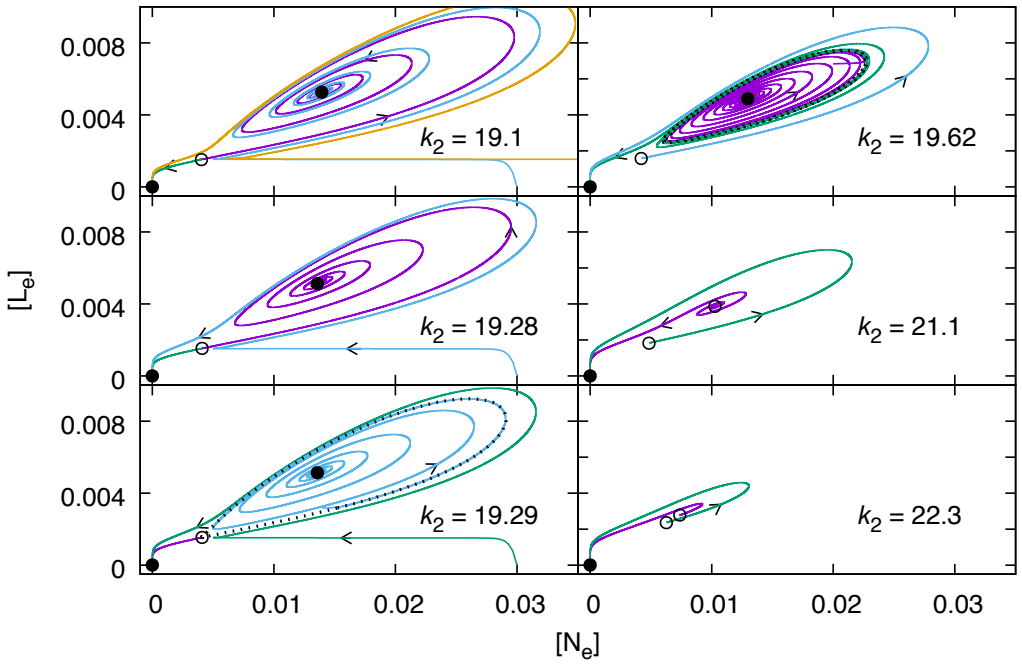

Figure 19: Phase portraits corresponding to several points in the bifurcation diagram presented in Fig. 18. Solid dots mark the stable equilibria, while open circles mark the unstable equilibria. Arrows show the direction of motion along the trajectories, with different trajectories distinguished by color. The gold-colored curve at $k_2 = 19.1$ was started from $[\mathrm{N_e}] = 0.06$, outside the frame of the figure. This trajectory approaches the saddle point, then makes an excursion all the way around the basin of attraction of the stable focus, briefly exiting the frame, and finally approaches the low-Nodal steady state. At $k_2 = 19.29$, the closed dotted curve is a homoclinic orbit connecting the unstable equilibrium point to itself, while at $k_2 = 19.62$, the closed dotted curve is an unstable limit cycle.

larger values of k_2 (e.g. $k_2 = 19.62$), this closed orbit detaches from the saddle point and becomes an unstable limit cycle. The limit cycle decreases in size as k_2 increases, its radius going to zero at the Andronov-Hopf bifurcation. Thereafter (e.g. at $k_2 = 21.1$), the high-Nodal steady state becomes an unstable focus. The final panel of Fig. 19 shows trajectories in the vicinity of the steady states just before the two unstable steady states collide at the saddle-node bifurcation.

The two bifurcation diagrams shown in Figs. 15 and 18 differ only in their values of k_1. We can see the connection between them by computing a phase diagram showing the bifurcation curves in parameter space, pre-

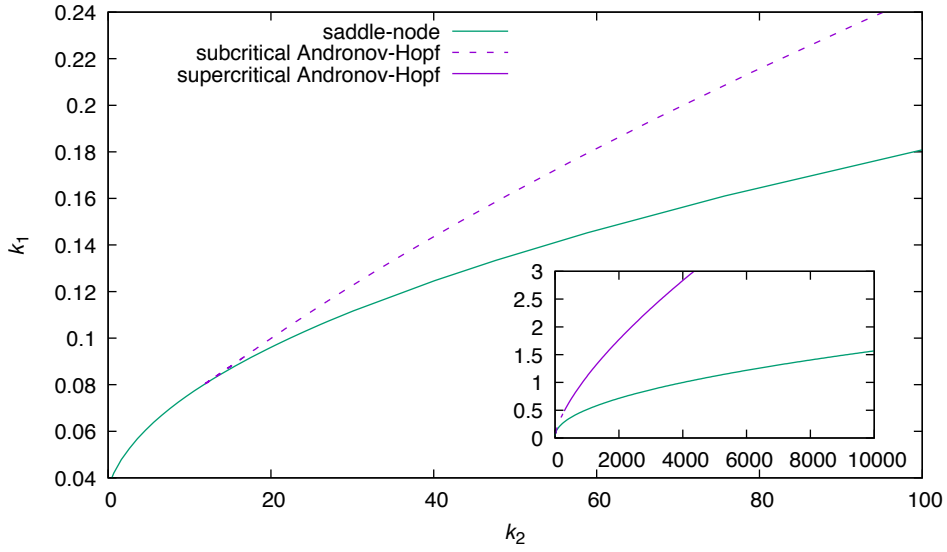

Figure 20: Phase diagram for the parameters of Figs. 15 and 18. The inset shows the phase diagram computed over a wider range of parameter values.

sented in Fig. 20. The Andronov-Hopf bifurcation curve connects the two points in the (k_2, k_1) plane corresponding to the Andronov-Hopf bifurcations in Figs. 15 and 18, roughly $(857.34, 1)$ and $(20.06, 0.1)$, respectively. Near $(284.67, 0.482)$, the bifurcation changes from a subcritical to a supercritical Andronov-Hopf bifurcation. Bistability occurs at parameter sets that lie above both the Andronov-Hopf and saddle-node bifurcation curves. Below the saddle-node curve, only the low-Nodal steady state exists. Between the Andronov-Hopf and saddle-node curves, the system has two unstable and one stable steady state. The two bifurcation curves meet at a Takens-Bogdanov point. A homoclinic bifurcation curve also emanates from this point, but it lies so near the Andronov-Hopf curve that the two cannot be distinguished on the scale of this figure.

6. Discussion and conclusions

6.1. Summary of results and conclusions

We have seen that Nodal alone is sufficient for bistability in a single cell governed by the biochemical network described in section 2. From the anal-

ysis of section 4.3, we can identify the key reactions that generate bistability in this model:

1. Nodal binds to the receptor, activating its kinase domain.
2. Smad2 is phosphorylated by R_A.
3. Two units of PSmad2 form a complex with transcription-factor activity. Note that neither the binding of the PSmad2 dimer to Smad4 assumed in this model, nor the binding of the heterotrimer to FoxH1 which we did not consider, are dynamically necessary to generate bistability.
4. The transcription factor activates the *nodal* gene.
5. Active Nodal protein is produced.

These are the core elements for bistability around which a model for the development of left-right asymmetry can be built. Other reactions may be required for structural stability, such as the direct dephosphorylation of PSmad2 [reaction (5)], but the key dynamical elements are those enumerated above.

We have focused on the bistable case because, in the absence of spatial variation in parameters, bistability provides necessary (but not sufficient) conditions for wave propagation. Moreover, a reaction mechanism that contains a critical fragment making bistability possible also meets a necessary condition for Turing patterning (Mincheva and Roussel, 2006).

Given the Hill-function kinetics assumed by Middleton et al. (2013), as well as the saturable kinetics for Smad2 phosphorylation in both their model and ours, one can ask whether saturability of any of the reactions in the model is critical. We found in section 4.3 that the model maintains a bistable regime even if we eliminate all sources of saturability. We reached these conclusions in part using a graph-theoretical method (Mincheva and Roussel, 2007), which often enabled us to determine that the network retained the key ingredients for bistability without doing any calculations beyond the initial identification of the critical fragment. We did find that eliminating saturability at the promoter tended to decrease the size of the basin of attraction of the low-Nodal steady state, so saturability remains important quantitatively, even though it is not critical to the qualitative behavior.

In order for different developmental fates to be selectable, the steady states corresponding to different fates must each have reasonably large basins

of attraction, and the system needs to be responsive to each important morphogen. Thus, the case shown in Fig. 6 is ideal: with a basin boundary that runs near the line $[L_e]_0 = [N_e]_0$ provided $[L_e]_0$ is not too small, the system will tend to reach the high-Nodal steady state when Nodal is in excess, and the low-Nodal state when Lefty is in excess. This makes steady state selection a relatively simple matter, roughly speaking because we have two "control knobs" that allow us to direct the system towards a desired steady state. On the other hand, the case shown in Fig. 7 makes for a much more difficult developmental fate selection problem: to reach the low-Nodal state, the Nodal concentration has to be carefully controlled because of the narrow basin of attraction of this state; moreover, Lefty is ineffective except at relatively low Nodal concentrations because of the steepness of the basin boundary. We note in passing that we have seen even steeper boundaries in some of our calculations, such as in Fig 14(b). While the basin calculations carried out here do not directly reflect what happens during normal development, they do suggest one possible role for Lefty, namely to facilitate the selection of a steady state given a particular history of a region of the developing tissue, and a particular context created by the surrounding cells.

At least for the parameter regions explored here, uncompetitive inhibition by intracellular Lefty alone, even when the parameters are tuned to increase the importance of the uncompetitive pathway, results in a system that is strikingly insensitive to Lefty (Fig. 14). We included uncompetitive inhibition in this model based on the experiments of Ulloa and Tabibzadeh (2001) with cultured cells which, to our knowledge, have not been replicated. Because negative results are seldom published, it may be that the result is simply irreproducible in other cell types and/or in embryos. However, there are two other possibilities to consider, one of which is that we may simply be exploring the wrong parameter regime. Given the number of parameters of the model, some doubt on this point may always remain. The other possibility is that intracellular Lefty really does inhibit the kinase activity of the Nodal receptor, but that because of the insensitivity of Nodal signaling to this intracellular inhibition, it has no real effect *in vivo*. If so, one has to wonder whether the intracellular uncompetitive inhibition is a simple side-effect of some other process involving Lefty since it would be difficult to imagine that evolution would maintain this function of Lefty otherwise. Tentatively, we conclude that the key mechanism for feedback inhibition by Lefty is the competitive inhibition at the extracellular binding site of the receptor. This agrees with the study of Middleton et al. (2013), who examined the alter-

native possibility suggested by Chen and Shen (2004) that Lefty and Nodal form an inhibitory complex, and found that the latter mode of inhibition required very particular biochemical conditions which were unlikely to prevail in practice.

Our results also show that the existence of the bistable regime in our model depends on tight control of *nodal* expression. This requires both that the *nodal* gene have a very low level of expression in the absence of the appropriate transcription factor, and that the accidental assembly of *nodal* transcription factors on the right-hand side of the embryo be a rare event. The latter is hardly guaranteed given the large number of developmental pathways in which all of the components, particularly the Smads (Hill, 2016) and Nodal, participate (Schier, 2003). It may well be that some of the additional factors not included in our model, notably Nodal antagonists of the Cerberus/DAN family, including Cerl (Schier, 2003), are required at least in part to minimize leaky expression of *nodal*.

6.2. Scenarios for left-right patterning

The model studied here displays bistability over a wide range of parameters, which should support left-right pattern formation. Middleton et al. (2013) have suggested that pattern formation in a very similar model to ours arises by "wave pinning". Wave pinning has been used to describe a variety of different dynamical phenomena. Historically, wave pinning was mostly used to describe the attachment of a wave to inhomogeneities in a medium or to defects in the container, a usage that goes back at least to the early 1990s (Nettesheim et al., 1993; Bär et al., 1994). Matthies and Wayne (2006) have used the term wave pinning in the closely related sense of propagation failure in an inhomogeneous medium. In the work of Mori et al. (2008), wave pinning is a phenomenon in which wave propagation stalls due to the exhaustion of a diffusible, nonrenewable precursor. Leaving aside attachment of a wave to a defect, what the latter two quite different mechanisms for wave pinning have in common is that the distance the wave travels before pinning is predictable. In the case of propagation failure in an inhomogeneous medium, the spatial profile of the inhomogeneities determines the distance of travel, while in the systems studied by Mori et al. (2008), exhaustion of the precursor causes the wave to stop. Neither of these is the mechanism associated with the halting of wave propagation in the Middleton et al. (2013) model. Rather, Middleton et al. (2013) observe wave propagation failure associated with the discreteness (i.e. cellularity) of the space (Keener, 1987). This is

quite different than situations typically described using the term wave pinning, since the location where the wave stops can depend in a complicated way on the initial conditions and history of the system (Fáth and Domański, 1999). From a developmental perspective, this mechanism for generating two distinct domains would seem to lack robustness, although this issue has not, to our knowledge, been carefully studied.

The history dependence of propagation failure may nevertheless allow this mechanism to be effective in developing the left-right pattern as it makes future pattern formation dependent on past developmental events. A suitable pre-pattern may therefore provide both the initial conditions and preconditions for predictable stopping required. Propagation failure is not the only tenable mechanism for pattern formation that depends on pre-patterning. Wave pinning by spatially inhomogeneous parameters similarly depends on pre-patterning. (But note that we do not know if the wave would become unpinned once the pre-pattern dissipates.)

At the stage at which Nodal and Lefty become active in left-right patterning, the embryo is not a featureless body. Among other things, there is a distinct midline which is known to play an important role in separating the left and right sides of the embryo (Shiratori and Hamada, 2006). Specifically, Lefty1 is expressed in the midline and acts as a barrier to spread of the high-Nodal state into the right side of the embryo (Meno et al., 1998). Moreover, the *lefty1* gene is expressed slightly earlier than *lefty2*. The midline clearly behaves differently than the surrounding tissue, presumably due to its own developmental history, i.e. pre-patterning of the midline establishes conditions for the confinement of the high-Nodal state to the left. The *nodal-lefty2* feedback loop would then play a smaller role in left-right patterning, contrary to the assumption of the Turing model (Juan and Hamada, 2001; Nakamura et al., 2006; Müller et al., 2012), but in accordance with the recent experimental results of Rogers et al. (2017).

As was recognized by Turing (1952), Turing patterns are also history-dependent as the Turing instability, in the absence of a clear initial asymmetry, can equally well result in the normal placement (*situs solitus*) as in the inverted placement (*situs inversus*) of the left and right domains. The initial conditions, i.e. the developmental history of the embryo, are critical to the reproducible placement of the organs. Whether the critical pre-patterning event is the cilia-driven nodal flow (Spéder et al., 2007) or the prior synthesis of the Nodal antagonist Cerl (or another protein of the Cerberus/DAN family) on the right side of the embryo (Kawasumi et al., 2011) [which has

itself been the subject of modeling (Nakamura et al., 2012)] is a matter for further research.

Regarding the experiments of Rogers et al. (2017) mentioned above, it should be mentioned that these results were obtained in zebrafish. It will be interesting to know if they can be replicated in other organisms, especially in mammals. In the meantime, a spatio-temporal version of the present model could be used to explore various scenarios for pattern formation, with and without involvement of the midline as a distinct structure, with and without *nodal-lefty* feedback, etc.

6.3. Future model development

The present model leaves out many interesting biochemical details whose exact roles are not well understood. Rather than present a laundry list of potential extensions, we focus here on a few that we think are particularly interesting, in addition to the issues surrounding the role of the midline and of Cerl mentioned above.

Reactions (1) to (4) of the model are a cartoon, as the receptor dynamics are much more interesting. An EGF-CFC coreceptor (Cripto or related proteins) binds Nodal first (Shiratori and Hamada, 2014). Cripto assists the binding of Nodal to the type I receptor (Acvr1b) (Sakuma et al., 2002; Schier, 2003) with subsequent addition of the type II receptor (Acvr2a or Acvr2b) to the complex (Reissmann et al., 2001; Schier, 2009). Acvr2a/b phosphorylates Acvr1b, activating the latter as a kinase for the R-Smads. The R-Smads are activated by phosphorylation at two serine residues by the Acvr1b kinase (Souchelnytskyi et al., 1997). The receptors are eventually internalized and recycled (Constam, 2009; Wei and Wang, 2018). These interactions are replete with nonlinearities, any of which might enhance the tendency of this network to generate bistability, or significantly shift the basins of attraction of the two steady states, among other possibilities.

As a byproduct of elaborating the receptor model, we would be able to correctly model the mechanism of inhibition of Nodal signaling by Lefty. The weight of evidence suggests that Lefty does not bind to the Activin receptors, but to the coreceptor Cripto (Cheng et al., 2004; Chen and Shen, 2004; Branford and Yost, 2004), although there is not unanimity on this point (Sakuma et al., 2002; Shiratori and Hamada, 2014). There is no reason to believe that this subtlety would have a major effect on the behavior of a model of left-right development. Nevertheless, it would be preferable to model the mechanism of inhibition realistically as this may affect the behavior of more

complex models that take into account the cross-talk between various TGF-β signals.

Processing of the Nodal precursor and subsequent dimerization is essential for Nodal function (Le Good et al., 2005; Constam, 2009; Tessadori et al., 2015). Interestingly, Cripto is likely involved in these steps as well (Blanchet et al., 2008; Constam, 2009). These steps are particularly interesting in that the bimolecular dimerization step might increase the order of the feedback in the autocatalytic loop. It is not impossible that considering dimerization of Nodal might allow bistability with a single Smad2 in the transcription factor complex. The plausibility of this biochemical hypothesis could be studied using a critical fragment analysis of a model built for the purpose.

DRAP1 has paradoxical roles in the control of the Nodal-Lefty system (Iratni et al., 2002): It binds FoxH1, preventing it from binding DNA. This function of DRAP1 should reduce the levels of both Nodal and Lefty2 expression. On the other hand, DRAP1 also seems to be required for Lefty2 expression. Developing models that account for these observations may help direct experimental investigations. Moreover, the complex regulatory interactions between Nodal, Lefty2 and DRAP1 implied by the foregoing observations suggest a dynamically interesting role for DRAP1.

Paradoxically, while there is a great deal of biochemistry yet to be added to the model, it may be that the greatest gains come from a rigorous simplification of the model. If the dynamics can be reduced to two or three variables, powerful analytic tools can be applied to fully understand the behavior in time and space. Some of our results suggest possible reductions, e.g. the reduction of reactions (3) and (4) to a simple bimolecular process. A combination of rigorous model simplification and of the judicious addition of interesting biochemical interactions will likely prove to be a fruitful approach, especially for the study of the spatio-temporal development of asymmetry.

6.4. Concluding comments

We now have a model built entirely from realistic chemical reactions that displays bistability across a wide range of parameters. Our model supports a transcription factor stoichiometry that includes two molecules of phosphorylated Smad2, as suggested by Inman and Hill (2002) and by Hill (2016). Our modeling results suggest that there is no role for uncompetitive inhibition by internalized Lefty2, contrary to the study of Ulloa and Tabibzadeh (2001). Finally, our work suggests that Lefty2 might play a role in facilitating the

selection of a steady state, but not in the basic mechanism of bistability, which is consistent with the recent study of Rogers et al. (2017).

The latter finding is intriguing. What is the dynamical role, or roles, of Lefty? Steady-state selection is certainly one possible role. It is also likely that Lefty is required for pattern formation by the usual long-range inhibition mechanism (Meinhardt and Gierer, 2000; Sakuma et al., 2002), although recent experimental evidence in zebrafish suggests otherwise (Rogers et al., 2017). Does Lefty mostly tune the level of Nodal, as suggested by Rogers et al. (2017)? Or does it play a kinetic role, for instance by reducing the time required to reach the steady state, as has been seen in other systems with negative feedback (Rosenfeld et al., 2002)? Unraveling these questions will require a combination of theoretical and experimental studies.

Acknowledgements

A preliminary model which eventually evolved into the model presented here was developed in association with Lekhnath Ghimire, whose contribution we gratefully acknowledge. We also wish to thank the anonymous referee whose detailed comments substantially improved this paper. This work was funded by the Natural Sciences and Engineering Research Council of Canada, and by the University of Lethbridge.

References

References

Alvarez, J., Serra, R., 2004. Unique and redundant roles of Smad3 in TGF-β-mediated regulation of long bone development in organ culture. Dev. Dyn. 230, 685–699.

Andronov, A., Pontrjagin, L., 1937. Systèmes grossiers. C. R. Acad. Sci. URSS 14, 247–250.

Bär, M., Gottschalk, N., Eiswirth, M., Ertl, G., 1994. Spiral waves in a surface reaction: Model calculations. J. Chem. Phys. 100, 1202–1214.

Besser, D., 2004. Expression of Nodal, Lefty-A, and Lefty-B in undifferentiated human embryonic stem cells requires activation of Smad2/3. J. Biol. Chem. 279, 45076–45084.

Blanchet, M.-H., Le Good, J. A., Mesnard, D., Oorschot, V., Baflast, S., Minchiotti, G., Klumperman, J., Constam, D. B., 2008. Cripto recruits Furin and PACE4 and controls Nodal trafficking during proteolytic maturation. EMBO J. 27, 2580–2591.

Branford, W. W., Yost, H. J., 2004. Nodal signaling: Cryptic Lefty mechanism of antagonism decoded. Curr. Biol. 14, R341–R343.

Briggs, W. E., 1985. Zeros and factors of polynomials with positive coefficients and protein-ligand binding. Rocky Mountain J. Math. 15, 75–89.

Brown, K. A., Pietenpol, J. A., Moses, H. L., 2007. A tale of two proteins: Differential roles and regulation of Smad2 and Smad3 in TGF-β signaling. J. Cell. Biochem. 101, 9–33.

Capdevila, J., Vogan, K. J., Tabin, C. J., Izpisúa Belmonte, J. C., 2000. Mechanisms of left-right determination in vertebrates. Cell 101, 9–21.

Chen, C., Shen, M. M., 2004. Two modes by which Lefty proteins inhibit Nodal signaling. Curr. Biol. 14, 618–624.

Cheng, S. K., Olale, F., Brivanlou, A. H., Schier, A. F., 2004. Lefty blocks a subset of TGFβ signals by antagonizing EGF-CFC coreceptors. PLoS Biol. 2, e30.

Ciechanover, A., Orian, A., Schwartz, A. L., 2000. Ubiquitin-mediated proteolysis: Biological regulation via destruction. BioEssays 22, 442–451.

Clarke, B. L., 1974. Graph theoretic approach to the stability analysis of steady state chemical reaction networks. J. Chem. Phys. 60, 1481–1492.

Constam, D. B., 2009. Running the gauntlet: an overview of the modalities of travel employed by the putative morphogen Nodal. Curr. Opin. Genet. Dev. 19, 302–307.

Edelstein, B. B., 1970. Biochemical model with multiple steady states and hysteresis. J. Theor. Biol. 29, 57–62.

Ermakov, G. L., 2003. A theoretical graph method for search and analysis of critical phenomena in biochemical systems. I. Graphical rules for detecting oscillators. Biochemistry (Moscow) 68, 1109–1120.

Ermakov, G. L., Goldstein, B. N., 2002. Simplest kinetic schemes for biochemical oscillators. Biochemistry (Moscow) 67, 473–484.

Ermentrout, B., 2002. Simulating, Analyzing, and Animating Dynamical Systems. SIAM, Philadelphia.

Fáth, G., Domański, Z., 1999. Avalanche of bifurcations and hysteresis in a model of cellular differentiation. Phys. Rev. E 60, 4604–4609.

Feinberg, M., 1987. Chemical reaction network structure and the stability of complex isothermal reactors—I. The deficiency zero and deficiency one theorems. Chem. Eng. Sci. 42, 2229–2268.

Glass, L., Mackey, M. C., 1988. From Clocks to Chaos: The Rhythms of Life. Princeton University Press, Princeton.

Goldbeter, A., 1996. Biochemical Oscillations and Cellular Rhythms. Cambridge University Press, Cambridge.

Goldstein, B. N., Ermakov, G., Centelles, J. J., Westerhoff, H. V., Cascante, M., 2004. What makes biochemical networks tick? A graphical tool for the identification of oscillophores. Eur. J. Biochem. 271, 3877–3887.

Guckenheimer, J., Holmes, P., 1990. Nonlinear Oscillations, Dynamical Systems, and Bifurcations of Vector Fields. Springer, New York.

Hale, J. K., Koçak, H., 1991. Dynamics and Bifurcations. Vol. 3 of Texts in Applied Mathematics. Springer, New York.

Hamada, H., Meno, C., Saijoh, Y., Adachi, H., Yashiro, K., Sakuma, R., Shiratori, H., 2001. Role of asymmetric signals in left-right patterning in the mouse. Am. J. Med. Genet. 101, 324–327.

Hill, C. S., 2016. Transcriptional Control by the SMADs. Cold Spring Harb. Perspect. Biol. 8, a022079.

Inman, G. J., Hill, C. S., 2002. Stoichiometry of active Smad-transcription factor complexes on DNA. J. Biol. Chem. 277, 51008–51016.

Iratni, R., Yan, Y.-T., Chen, C., Ding, J., Zhang, Y., Price, S. M., Reinberg, D., Shen, M. M., 2002. Inhibition of excess Nodal signaling during mouse gastrulation by the transcriptional corepressor DRAP1. Science 298, 1996–1999.

Ivanova, A. N., 1979. Conditions for uniqueness of the stationary states of kinetic systems, connected with the structures of their reaction mechanisms. I. Kinet. Catal. 20, 833–837.

Ivanova, A. N., Tarnopol'skii, B. L., 1979. One approach to the determination of a number of qualitative features in the behavior of kinetic systems, and realization of this approach in a computer (critical conditions, autooscillations). Kinet. Catal. 20, 1271–1277.

Juan, H., Hamada, H., 2001. Roles of *nodal-lefty* regulatory loops in embryonic patterning of vertebrates. Genes Cells 6, 923–930.

Kawasumi, A., Nakamura, T., Iwai, N., Yashiro, K., Saijoh, Y., Belo, J. A., Shiratori, H., Hamada, H., 2011. Left-right asymmetry in the level of active Nodal protein produced in the node is translated into left-right asymmetry in the lateral plate of mouse embryos. Dev. Biol. 353, 321–330.

Keener, J. P., 1987. Propagation and its failure in coupled systems of discrete excitable cells. SIAM J. Appl. Math. 47, 556–572.

Le Good, J. A., Joubin, K., Giraldez, A. J., Ben-Haim, N., Beck, S., Chen, Y., Schier, A. F., Constam, D. B., 2005. Nodal stability determines signaling range. Curr. Biol. 15, 31–36.

Lewis, J., Slack, J. M. W., Wolpert, L., 1977. Thresholds in development. J. Theor. Biol. 65, 579–590.

Li, N., Yang, Y., He, K., Zhang, F., Zhao, L., Zhou, W., Yuan, J., Liang, W., Fang, X., 2016. Single-molecule imaging reveals the activation dynamics of intracellular protein Smad3 on cell membrane. Sci. Rep. 6, 33469.

Mackey, M. C., Santillán, M., Tyran-Kamińska, M., Zeron, E. S., 2016. Simple Mathematical Models of Gene Regulatory Dynamics. Springer, Cham, Switzerland.

Marcellini, S., 2006. When Brachyury meets Smad1: The evolution of bilateral symmetry during gastrulation. BioEssays 28, 413–420.

Massagué, J., Seoane, J., Wotton, D., 2005. Smad transcription factors. Genes Dev. 19, 2783–2810.

1174 Matthies, K., Wayne, C. E., 2006. Wave pinning in strips. Proc. Roy. Soc.
1175 Edinburgh Sect. A 136, 971–995.

1176 Meinhardt, H., Gierer, A., 2000. Pattern formation by local self-activation
1177 and lateral inhibition. BioEssays 22, 753–760.

1178 Meno, C., Gritsman, K., Ohishi, S., Ohfuji, Y., Heckscher, E., Mochida,
1179 K., Shimono, A., Kondoh, H., Talbot, W. S., Robertson, E. J., Schier,
1180 A. F., Hamada, H., 1999. Mouse Lefty2 and zebrafish Antivin are feedback
1181 inhibitors of Nodal signaling during vertebrate gastrulation. Mol. Cell 4,
1182 287–298.

1183 Meno, C., Saijoh, Y., Fujii, H., Ikeda, M., Yokoyama, T., Yokoyama, M.,
1184 Toyoda, Y., Hamada, H., 1996. Left-right asymmetric expression of the
1185 TGFβ-family member *lefty* in mouse embryos. Nature 381, 151–155.

1186 Meno, C., Shimono, A., Saijoh, Y., Yashiro, K., Mochida, K., Ohishi, S.,
1187 Noji, S., Kondoh, H., Hamada, H., 1998. *lefty-1* is required for left-right
1188 determination as a regulator of *lefty-2* and *nodal*. Cell 94, 287–297.

1189 Middleton, A. M., King, J. R., Loose, M., 2013. Wave pinning and spatial
1190 patterning in a mathematical model of Antivin/Lefty-Nodal signalling. J.
1191 Math. Biol. 67, 1393–1424.

1192 Mincheva, M., Roussel, M. R., 2006. A graph-theoretic method for detecting
1193 potential Turing bifurcations. J. Chem. Phys. 125, 204102.

1194 Mincheva, M., Roussel, M. R., 2007. Graph-theoretic methods for the analy-
1195 sis of chemical and biochemical networks. I. Multistability and oscillations
1196 in ordinary differential equation models. J. Math. Biol. 55, 61–86.

1197 Mori, Y., Jilkine, A., Edelstein-Keshet, L., 2008. Wave-pinning and cell po-
1198 larity from a bistable reaction-diffusion system. Biophys. J. 94, 3684–3697.

1199 Müller, P., Rogers, K. W., Jordan, B. M., Lee, J. S., Robson, D., Ra-
1200 manathan, S., Schier, A. F., 2012. Differential diffusivity of Nodal and
1201 Lefty underlies a reaction-diffusion patterning system. Science 336, 721–
1202 724.

1203 Murray, J. D., 2002. Mathematical Biology I: An Introduction, 3rd Edition.
1204 Springer, New York.

Nakamura, T., Hamada, H., 2012. Left-right patterning: conserved and divergent mechanisms. Development 139, 3257–3262.

Nakamura, T., Mine, N., Nakaguchi, E., Mochizuki, A., Yamamoto, M., Yashiro, K., Meno, C., Hamada, H., 2006. Generation of robust left-right asymmetry in the mouse embryo requires a self-enhancement and lateral-inhibition system. Dev. Cell 11, 495–504.

Nakamura, T., Saito, D., Kawasumi, A., Shinohara, K., Asai, Y., Takaoka, K., Dong, F., Takamatsu, A., Belo, J. A., Mochizuki, A., Hamada, H., 2012. Fluid flow and interlinked feedback loops establish left-right asymmetric decay of *Cerl2* mRNA. Nat. Commun. 3, 1322.

Nettesheim, S., von Oertzen, A., Rotermund, H. H., Ertl, G., 1993. Reaction diffusion patterns in the catalytic CO-oxidation on Pt(110): Front propagation and spiral waves. J. Chem. Phys. 98, 9977–9985.

Ngo, L. G., Roussel, M. R., 1997. A new class of biochemical oscillator models based on competitive binding. Eur. J. Biochem. 245, 182–190.

Quirk, J., Ruppert, R., 1965. Qualitative economics and the stability of equilibrium. Rev. Econ. Studies 32, 311–326.

Ramsdell, A. F., Yost, H. J., 1998. Molecular mechanisms of vertebrate left-right development. Trends Genet. 14, 459–465.

Reissmann, E., Jörnvall, H., Blokzijl, A., Andersson, O., Chang, C., Minchiotti, G., Persico, M. G., Ibáñez, C. F., Brivanlou, A. H., 2001. The orphan receptor ALK7 and the activin receptor ALK4 mediate signaling by Nodal proteins during vertebrate development. Genes Dev. 15, 2010–2022.

Rinzel, J., Terman, D., 1982. Propagation phenomena in a bistable reaction-diffusion system. SIAM J. Appl. Math. 42, 1111–1137.

Rogers, K. W., Lord, N. D., Gagnon, J. A., Pauli, A., Zimmerman, S., Aksel, D. C., Reyon, D., Tsai, S. Q., Joung, J. K., Schier, A. F., 2017. Nodal patterning without Lefty inhibitory feedback is functional but fragile. eLife 6, e28785.

Rosenfeld, N., Elowitz, M. B., Alon, U., 2002. Negative autoregulation speeds the response times of transcription networks. J. Mol. Biol. 323, 785–793.

Ross, S., Hill, C. S., 2008. How the Smads regulate transcription. Int. J. Biochem. Cell Biol. 40, 383–408.

Sakuma, R., Ohnishi, Y., Meno, C., Fujii, H., Juan, H., Takeuchi, J., Ogura, T., Li, E., Miyazono, K., Hamada, H., 2002. Inhibition of Nodal signalling by Lefty mediated through interaction with common receptors and efficient diffusion. Genes Cells 7, 401–412.

Schier, A. F., 2003. Nodal signaling in vertebrate development. Annu. Rev. Cell Dev. Biol. 19, 589–621.

Schier, A. F., 2009. Nodal morphogens. Cold Spring Harb. Perspect. Biol. 1, a003459.

Schmierer, B., Tournier, A. L., Bates, P. A., Hill, C. S., 2008. Mathematical modeling identifies Smad nucleocytoplasmic shuttling as a dynamic signal-interpreting system. Proc. Natl. Acad. Sci. U.S.A. 105, 6608–6613.

Shen, M. M., 2007. Nodal signaling: developmental roles and regulation. Development 134, 1023–1034.

Shiratori, H., Hamada, H., 2006. The left-right axis in the mouse: from origin to morphology. Development 133, 2095–2104.

Shiratori, H., Hamada, H., 2014. TGFβ signaling in establishing left-right asymmetry. Semin. Cell Dev. Biol. 32, 80–84.

Souchelnytskyi, S., Tamaki, K., Engström, U., Wernstedt, C., ten Dijke, P., Heldin, C.-H., 1997. Phosphorylation of Ser^{465} and Ser^{467} in the C terminus of Smad2 mediates interaction with Smad4 and is required for transforming growth factor-β signaling. J. Biol. Chem. 272, 28107–28115.

Spéder, P., Petzoldt, A., Suzanne, M., Noselli, S., 2007. Strategies to establish left/right asymmetry in vertebrates and invertebrates. Curr. Opin. Genet. Dev. 17, 351–358.

Strogatz, S. H., 1994. Nonlinear Dynamics and Chaos. Westview Press, Cambridge, Massachusetts.

Tessadori, F., Noël, E. S., Rens, E. G., Magliozzi, R., Evers-van Gogh, I. J. A., Guardavaccaro, D., Merks, R. M. H., Bakkers, J., 2015. Nodal signaling range is regulated by proprotein convertase-mediated maturation. Dev. Cell 32, 631–639.

Thom, R., 1975. Structural Stability and Morphogenesis. W. A. Benjamin, Reading, Massachusetts.

Thomas, R., Kaufman, M., 2001. Multistationarity, the basis of cell differentiation and memory. I. Structural conditions of multistationarity and other nontrivial behavior. Chaos 11, 170–179.

Turing, A. M., 1952. The chemical basis of morphogenesis. Philos. Trans. R. Soc. London, Ser. B 237, 37–72.

Ulloa, L., Creemers, J. W. M., Roy, S., Liu, S., Mason, J., Tabibzadeh, S., 2001. Lefty proteins exhibit unique processing and activate the MAPK pathway. J. Biol. Chem. 276, 21387–21396.

Ulloa, L., Tabibzadeh, S., 2001. Lefty inhibits receptor-regulated Smad phosphorylation induced by the activated transforming growth factor-β receptor. J. Biol. Chem. 276, 21397–21404.

Vandenberg, L. N., Levin, M., 2013. A unified model for left-right asymmetry? Comparison and synthesis of molecular models of embryonic laterality. Dev. Biol. 379, 1–15.

Walther, G. R., Hartley, M., Mincheva, M., 2014. GraTeLPy: Graph-theoretic linear stability analysis. BMC Syst. Biol. 8, 22.

Wei, S., Wang, Q., 2018. Molecular regulation of Nodal signaling during mesendoderm formation. Acta Biochim. Biophys. Sin. 50, 74–81.